Formulation and Characterization of Bio-Enhanced Thermoset Resin Composites for Additive Manufacturing

by

Laura Vanessa Alvarez Marin

A thesis submitted to the Graduate Faculty of
Auburn University
in partial fulfillment of the
requirements for the Degree of
Master of Science

Auburn, Alabama
August 9, 2025

Key words: Thermoset Resins, Additive Manufacturing,
Sustainable Construction Materials

Approved by

Dr. Maria Soledad Peresin, Professor, College of Forestry, Wildlife, and Environment
Dr. Brian K. Via, Professor, College of Forestry, Wildlife, and Environment
Dr. Michael Maughan, Professor, Department of Mechanical Engineering

Abstract

The transition to sustainable construction materials is essential to reducing the environmental footprint of the building industry. This research project aims to develop, characterize, and optimize thermoset biocomposite materials for use in additive manufacturing—specifically, 3D printing of structural housing components. By integrating renewable fillers and partially bio-based resin matrices, the project proposes novel composite formulations that meet the dual demand for high performance and environmental responsibility. The research was structured in three complementary studies. The first focused on enhancing epoxy resin with cellulose nanofibers (CNFs) derived from both bleached and lignin-containing pulp, to assess how residual lignin influences reinforcement efficiency. It was found that 0.75 wt% bleached CNF significantly improved composite toughness (41%) and stiffness (79%), while lignin-containing CNFs, although mechanically less effective, contributed to thermal stability through their antioxidant nature. The second study addressed the processability of bio-filled epoxy composites by optimizing extrusion parameters for wood flour–epoxy systems. Using a factorial design, the effects of particle size, wood content, and extrusion rate were evaluated. A 55:45 epoxy-to-wood ratio was identified as optimal, yielding composites with superior mechanical performance, dimensional stability, and fire resistance—confirming their suitability for extrusion-based 3D printing applications.

To further enhance the sustainability of the matrix itself, the third study investigated the partial replacement of petroleum-derived phenol in phenol-resorcinol-formaldehyde (PRF) resins with bio-oil obtained from the pyrolysis of waste wood. Substitution levels of up to 50% were tested, with 30% bio-oil replacement maintaining satisfactory flexural properties and curing behavior. Although 50% substitution led to a decrease in strength and stiffness, it introduced ductility and flexibility into the material. Thermal and curing behavior were shown to be tunable by adjusting the formulation and curing temperature. Together, these studies provide a holistic approach to the design of bio-based thermoset composites—from reinforcement and process optimization to resin sustainability. The findings demonstrate the feasibility of

creating high-performance, 3D-printable construction materials that align with the goals of carbon reduction, circular resource use, and sustainable development in the construction sector.

Acknowledgments

First and foremost, I want to thank God for blessing me with wonderful people who have supported my personal and professional growth.

I am deeply grateful to my advisor, Dr. M. Soledad Peresin, for this invaluable opportunity, for her academic, professional, and personal guidance, and for being an exceptional mentor from whom I have learned so much and whom I admire greatly. Her support has been fundamental throughout this journey. I would also like to thank Professor Germán Quintana from Universidad Pontificia Bolivariana for his recommendation and support at the beginning of this adventure.

I would also like to thank the members of my committee. To Dr. Zahra Naghizadeh, thank you for your patience, dedication, and for sharing your knowledge and support. To Dr. Brian K. Via, thank you for being an outstanding professor and mentor, always willing to help, and for allowing me to use your lab facilities to continue my research. To Dr. Michael Maughan, thank you for your constant support and guidance, and for the opportunity to be part of the PrinTimber project, which provided me with an enriching experience and the chance to engage in interdisciplinary collaboration with experts from different fields.

Special thanks to the resin team in the PrinTimber project: Dr. Maria Auad and Dr. Armando McDonald, for your continued guidance and feedback, and especially to Dr. Adhikari for generously sharing your knowledge and providing the bio-oil used in my experiments. I am sincerely grateful to all the faculty, staff, colleagues, and friends from the Sustainable Bio-Based Materials Lab and the College of Forestry, Wildlife and Environment. Your guidance, shared knowledge, and continuous support have been invaluable throughout this experience. I also want to thank the people who made this experience away from home more enjoyable—my friends in Auburn: Clara, Melissa, Laura, Abi, Christian, Kamila, and John. Thank you for your friendship and support.

Finally, I dedicate this thesis to my beloved family. To my parents, Carlos Alvarez and Sonia Marin, for their unconditional love and support, for leading by example, and always encouraging me to grow. To my siblings, Carlos Andrés and Kathy, for their love and for making me smile even from afar. To my dear grandmother Berta, for her endless affection. And to my fiancé, Carlos Montoya, thank you for your love, encouragement, and unwavering support. You have been my strength every step of the way.

Table of Contents

List of Tables

List of Figures

List of Abbreviations

3D	Three-dimensional
AFM	Atomic Force Microscopy
AM	Additive Manufacturing
BCNF	Bleached Cellulose Nanofibrils
BPR	Bio-Phenol Resin
CBO	Crude Bio-Oil
CNF	Cellulose Nanofibrils
D-400	Polyoxypropylene diamine
DLS	Dynamic Light Scattering
EP	Epoxy
FTIR	Fourier-Transform Infrared Spectroscopy
HexA	Hexenuronic Acids
LCNF	Lignin-Containing Cellulose Nanofibrils
PRF	Phenol-Resorcinol-Formaldehyde
QCM-D	Quartz Crystal Microbalance with Dissipation
SEM	Scanning Electron Microscopy

TGA	Thermogravimetric Analyzer
WPC	Wood-Plastic Composite
SYP	Southern Yellow Pine
DGEBA	Diglycidyl Ether of Bisphenol A
Epon 828	Commercial DGEBA epoxy resin
D-400	Polyoxypropylene diamine (Jeffamine D-400)
ASTM	American Society for Testing and Materials
ANOVA	Analysis of Variance
rpm	Revolutions per minute
IR	Infrared
WPC	Wood Plastic Composite
MOE	Modulus of Elasticity
SLM	Standard Liters per Minute
MOR	Modulus of Rupture
Tmax	Maximum Degradation Temperature

Chapter 1

General Overview

1.1 Introduction

In recent years, the development of additive manufacturing technologies, such as Three-dimensional (3D) printing, has revolutionized multiple industries, including construction (El-Sayegh et al., 2020; Pan et al., 2021; Saba et al., 2016). Construction 3D printing (C3DP) is an innovative technology aimed at automating traditional construction processes. Although there is no clear definition within the industry, it is described as an additive manufacturing technique capable of creating buildings or components directly from digital three-dimensional (3D) models, thereby minimizing human intervention and simplifying the supply chain in construction (Zuo et al., 2019; Wang et al., 2023). The possibility of manufacturing houses through 3D printing has garnered considerable interest as it offers innovative solutions to reduce costs, optimize material usage, and minimize construction times (Shahzad et al., 2021). However, one of the main challenges in this field is the search for materials that offer both structural strength and environmental sustainability.

To date, concrete has been the most widely used material in construction, both in traditional methods and additive manufacturing, due to its high mechanical strength, low production cost, local availability, and its versatility to be molded into various shapes, including those required for three-dimensional (3D) printing applications (Shahzad et al., 2021). Additionally, its thermal resistance, durability, and composition (15% cement, 25-30% fine aggregates, 70-75% coarse aggregates, and 22% water) contribute to its widespread use in construction. Its ease of adjusting viscosity and achieving appropriate yield strength further supports its role as an ideal material for 3D printing. However, this material is responsible for generating between 0.66 and 0.82 kg of CO2 per kilogram produced, accounting

for 7% of global emissions (Costa & Ribeiro, 2020). It is estimated that Portland cement consumption will reach 6 billion tons by 2060 (Felipe Arbeláez Pérez et al., 2024).

Given the global demand to reduce CO2 emissions in the construction industry (Benhelal et al., 2013; Miller et al., 2018), there is a need for innovative construction technologies that not only pave the way for a sustainable construction future but also reduce construction costs and facility management while providing a competitive advantage (Tay et al., 2017). The incorporation of wood waste and other lignocellulosic materials into additive manufacturing (AM) presents a promising strategy to reduce production costs and mitigate the environmental impact of construction processes (Krapež Tomec & Kariž, 2022). In the United States alone, sawmills generate substantial quantities of wood waste as a byproduct of timber processing. For example, it is estimated that approximately 83.4 million tons of primary timber wood and bark processing residues were produced in 2010, with nearly 98% of this material being recovered, combusted, or otherwise utilized (U.S. Environmental Protection Agency, 2018). While some of these residues are used in the manufacture of particle boards and fiberboards, the majority is still consumed for energy generation, representing a low-value end use. Despite the abundance of this renewable resource, its application in emerging AM technologies for construction remains largely unexplored (Carne et al., 2023).

Recent research has explored incorporating wood as a base material for filaments in AM by blending it with thermoplastic resins such as polylactic acid (PLA), acrylonitrile butadiene styrene (ABS), polyamide (nylon, PA), and polyether ether ketone (PEEK) (Dixit & Jain, 2020; Pop et al., 2019). However, the remelting capability of these thermoplastics limits the mechanical strength of the final materials, restricting their use to less demanding construction applications. Despite these limitations, leveraging lignocellulosic waste in advanced manufacturing technologies remains a high-potential research area for driving sustainable solutions in the industry.

For this reason, composite materials of thermosetting resins with wood, also known as thermoset biocomposites, combine the hardness and strength of resins with the renewable properties of wood (Yang et al., 2012). Among the most commonly used thermosetting resins are epoxy, phenolics, and urea-

formaldehyde, which are widely employed to enhance the physical properties of wood. These biocomposites have emerged as a promising alternative thanks to their unique combination of mechanical and thermal properties, making them an ideal solution for applications requiring strength, durability, and sustainability.

This research project aims to develop, characterize, and optimize particulate thermoset biocomposite materials tailored for 3D printing of sustainable housing components. The work explores the synergistic combination of thermoset matrices—epoxy and phenol-resorcinol-formaldehyde (PRF) resins—with lignocellulosic fillers and bio-based components derived from waste wood. Through a series of systematic studies, the project evaluates the mechanical, thermal, and processing performance of these bio-based composites.

1.2 Background

Currently, consumers, industries, and governments are increasingly prioritizing products made from renewable and sustainable resources. These products must be biodegradable, free of petroleum-derived components, carbon-neutral, and safe for both the environment and human health (Gardner & Wang, 2019). This shift is driven by growing awareness of environmental issues, the need to reduce carbon footprints, and stricter regulations aimed at promoting sustainable development and mitigating climate change.

Additive manufacturing, unlike traditional subtractive processes, enables the efficient creation of complex products and functional components with minimal waste and reduced production costs. However, significant advancements are still required to diversify material options and promote environmentally friendly solutions, as many of the materials currently used remain petroleum-derived (Krapež Tomec & Kariž, 2022). In this context, wood-plastic composites (WPCs) represent a promising alternative for replacing traditional materials like cement while leveraging renewable resources such as wood. Wood offers low density, low cost, and biodegradability, and when combined with plastics, its adhesive properties

as a matrix can be utilized (Hietala et al., 2011; Oksman & Clemons, 1998). This combination creates improved materials with high stiffness, increased ductility, and better impact resistance (Nygård et al., 2008). Currently, the most commonly used wood material in composites is wood flour, which consists of small wood particles with a relatively low aspect ratio obtained through milling. For composite products, the optimal wood flour particle size ranges from 180 to 425 μm (40 to 80 mesh sizes) (Pokhrel et al., 2021).

In the realm of composite materials, the most commonly used plastics are thermoplastics and thermosets. Thermoplastics are characterized by their ability to be melted and reshaped repeatedly due to their molecular bonds being formed through van der Waals forces. In contrast, thermosets cannot be remelted once cured because they form stable and irreversible chemical bonds, a distinction that stems from the extensive polymerization and cross-linking of their molecular chains (Zhang et al., 2024). This structural difference gives thermosets unique properties that are particularly advantageous in applications such as three-dimensional (3D) printing, where they significantly enhance interlayer adhesion, stiffness, and hardness of the fabricated components (Zhang et al., 2024). Thermosets include resins such as epoxy, phenolic, and urea-formaldehyde, which are widely used to improve the physical properties of wood, enhancing its durability, resistance to fungi and insects, and reducing moisture absorption (Yang et al., 2012).

The production of wood-plastic composites generally involves three main steps. The process begins with wood processing, which includes selecting the appropriate wood, drying it to reduce moisture content, milling (in the case of particulate composites), and sieving to obtain the desired particle size. Next, the wood flour is combined with the polymer matrix to create a homogeneous mixture. Finally, the composite is molded into final products using methods such as injection, extrusion, or compression molding, with extrusion being the most commonly used technique for wood-plastic composite manufacturing (Hietala et al., 2011; Ribeiro et al., 2023; Yang et al., 2012). Wood-plastic composites typically contain around 50% wood, and in some cases, as little as 30% (Clemons, Craig, 2002). This indicates that 50–70% of the material is still petroleum-based resin, which reflects a high dependence on petroleum-derived plastics.

One alternative to reduce the use of petroleum-based plastics is to partially replace these plastics with bio-based materials (Raquez et al., 2010). Renewable resources offer a promising, sustainable platform to substitute petroleum-based polymers, either partially or entirely. This is achievable by designing bio-based polymers that can compete with or even surpass existing petroleum-derived materials in cost-performance while offering high eco-friendliness (Kaplan, 1998). As a primary product of the fast pyrolysis of agricultural and forestry biomass, bio-oil is low-cost, renewable, and contains significant quantities of chemicals such as phenols, aldehydes, ketones, and acids (Xing et al., 2018). These characteristics position bio-oil as a potential replacement for traditional fossil-based materials in the preparation of bio-adhesives.

Recent studies have explored the partial replacement of petroleum-based thermoset resins with bio-oil for structural materials. Yu et al. (2018) developed a foaming bio-phenol resin (BPR) using bio-oil, phenol, and paraformaldehyde under alkaline conditions, achieving a 10.5–47.4% increase in compressive strength and a 25.0–50.5% increase in flexural strength with a 10–20% bio-oil substitution. Aslan et al. (2015) investigated the gradual replacement of commercial phenol-formaldehyde (PF) adhesive with up to 40 wt% of the phenol-rich fraction (PRF) of crude bio-oil (CBO), showing strong bonds at 10 wt% substitution. Bansode et al. (2021) studied lignin-derived bio-oils, demonstrating that a 50% replacement of phenol with kraft biorefinery lignin (L-KB) in novolac PF resin (50-NPF-L-KB) resulted in a tensile shear strength of 3.46 ± 0.55 MPa, outperforming other tested adhesives. Additionally, Asafu-Adjaye et al. (2022) evaluated bio-oil-based epoxy resin in oriented strand board (OSB) production, finding that up to 30% bio-oil substitution maintained feasible mechanical and water resistance properties. These findings highlight bio-oil's potential as a sustainable alternative in resin-based adhesives.

This thesis is carried out within the framework of the PrinTimber Project, which aims to advance sustainable construction by developing and implementing bio-based thermoset composite materials for use in additive manufacturing, specifically extrusion-based 3D printing of structural housing components. The core motivation of the PrinTimber Project is to reduce the environmental footprint of traditional building materials by partially replacing fossil-derived components with renewable resources while maintaining or

enhancing mechanical performance and processability. In this context, my research directly addresses critical aspects of material development by selecting specific renewable fillers and partially bio-based resin matrices, and by systematically studying their properties and suitability for additive manufacturing. The objectives and research questions defined in this thesis are therefore tailored to bridge existing knowledge gaps and provide data-driven insights needed for the practical implementation of biocomposite systems in 3D-printed housing applications. Further details of the experimental design and findings are discussed in the following chapters.

1.3 General Objective of Research

In line with this framework and the identified knowledge gaps, the general objective of this study is defined as follows:

To develop, characterize, and optimize thermoset biocomposite materials based on renewable fillers and partially bio-based resin matrices for their application in extrusion-based 3D printing of sustainable housing components, aiming to enhance mechanical performance, processability, and environmental sustainability in construction materials.

1.4 Chapter-Specific Objectives and hypotheses

1.4.1 Chapter 2

1.4.1.1 Hypothesis

The presence of residual lignin in cellulose nanofibrils (CNF) significantly influences their compatibility and reinforcing efficiency within epoxy matrices, and optimal loading levels exist for both

Lignin-Containing Cellulose Nanofibrils (LCNFs) and Bleached Cellulose Nanofibrils BCNF that maximize the mechanical and thermal performance of the resulting nanocomposites.

1.4.1.2 General Objective

To evaluate the effect of residual lignin in cellulose nanofibers on the mechanical, thermal, and interfacial properties of epoxy-based nanocomposites and identify optimal nanocellulose loading for enhanced composite performance.

1.4.1.3 Specific Objectives

- To characterize bleached (BCNF) and lignin-containing (LCNF) cellulose nanofibers in terms of morphology, surface charge, and chemical composition.
- To fabricate epoxy nanocomposites with varying loadings (0.5%, 0.75%, and 1%) of BCNF and LCNF.
- To evaluate and compare the mechanical properties (tensile strength, modulus, toughness, ductility) of BCNF- and LCNF-reinforced epoxy nanocomposites.
- To investigate the fiber–matrix interactions of CNFs with epoxy and curing agent through FTIR and Quartz Crystal Microbalance with Dissipation (QCM-D).
- To assess the thermal stability of the composites via thermogravimetric analysis (TGA) and evaluate the role of residual lignin in preserving thermal properties.
- To analyze the morphology of fractured surfaces using Scanning Electron Microscopy (SEM) to understand failure mechanisms and CNF dispersion.

1.4.2 Chapter 3

1.4.2.1 Hypothesis

Optimizing extrusion parameters—specifically wood flour particle size, screw speed, and epoxy-to-wood ratio—will significantly enhance the mechanical, physical, and fire-resistant properties of wood–epoxy composites, making them viable for use in extrusion-based additive manufacturing for construction applications.

1.4.2.2 General Objective

To optimize the extrusion parameters for the fabrication of wood flour–epoxy resin composites and evaluate their suitability for additive manufacturing applications in sustainable construction.

1.4.2.3 Specific Objectives

- To investigate the effect of wood flour particle size and screw speed on the extrudability and physical quality of wood–epoxy composite rods.
- To assess the impact of different epoxy-to-wood flour ratios on mechanical properties such as flexural and compressive strength.
- To evaluate water absorption and dimensional stability of the extruded composites under controlled immersion conditions.
- To perform fire resistance testing on the cured composite rods and analyze mass loss and thermal behavior during flame exposure.

1.4.3 Chapter 4

1.4.3.1 Hypothesis

Partial substitution of phenol with bio-oil in commercial phenol-resorcinol-formaldehyde (PRF) resin will modify the curing behavior and thermal properties of the adhesive, but up to a certain level, it will still maintain acceptable mechanical performance and allow for improved sustainability and processing flexibility.

1.4.3.2 General Objective

To investigate the effects of partially replacing commercial phenol-resorcinol-formaldehyde (PRF) resin with bio-oil on the thermal, curing, and mechanical properties of the adhesive system, and to identify optimal formulation and curing parameters for improved performance and sustainability.

1.4.3.3 Specific Objectives

- To determine the optimal bio-oil substitution level and curing conditions that balance sustainability with mechanical and thermal performance in PRF resin formulations.
- To analyze the curing behavior of the resin formulations using Differential Scanning Calorimetry (DSC) to identify thermal transitions and reaction profiles.
- To determine the gelation time of each formulation at different curing temperatures.
- To evaluate the thermal stability of cured resins via Thermogravimetric Analysis (TGA).
- To measure the flexural properties of the cured composites through three-point bending tests and assess the mechanical performance based on bio-oil content and curing temperature

1.5 References

Oksman, K., & Clemons, C. (1998). Mechanical properties and morphology of impact modified polypropylene-wood flour composites. *Journal of Applied Polymer Science*, *67*(9), 1503–1513. https://doi.org/10.1002/(SICI)1097-4628(19980228)67:9<1503::AID-APP1>3.0.CO;2-H

Raquez, J. M., Deléglise, M., Lacrampe, M. F., & Krawczak, P. (2010). Thermosetting (bio)materials derived from renewable resources: A critical review. In *Progress in Polymer Science (Oxford)* (Vol. 35, Issue 4, pp. 487–509). https://doi.org/10.1016/j.progpolymsci.2010.01.001

Kaplan, D.L. (1998). Introduction to Biopolymers from Renewable Resources. In: Kaplan, D.L. (eds) Biopolymers from Renewable Resources. Macromolecular Systems — Materials Approach. Springer, Berlin, Heidelberg. https://doi.org/10.1007/978-3-662-03680-8_1

Xing, J., Li, T., Yu, Y., Chen, C., & Chang, J. (2018). Development and characterization of a new bio-adhesive for wood using cassava starch and bio-oil. *International Journal of Adhesion and Adhesives*, *87*, 91–97. https://doi.org/10.1016/j.ijadhadh.2018.09.005

Yu, Y., Wang, Y., Xu, P., & Chang, J. (2018). Preparation and characterization of phenolic foam modified with bio-oil. *Materials*, *11*(11). https://doi.org/10.3390/ma11112228

Aslan, M., Özbay, G., & Ayrilmis, N. (2015). Adhesive characteristics and bonding performance of phenol formaldehyde modified with phenol-rich fraction of crude bio-oil. *Journal of Adhesion Science and Technology*, *29*(24), 2679–2691. https://doi.org/10.1080/01694243.2015.1080474

Nygård, P., Tanem, B. S., Karlsen, T., Brachet, P., & Leinsvang, B. (2008). Extrusion-based wood fibre-PP composites: Wood powder and pelletized wood fibres - a comparative study. *Composites Science and Technology*, *68*(15–16), 3418–3424. https://doi.org/10.1016/j.compscitech.2008.09.029

Pokhrel, G., Gardner, D. J., & Han, Y. (2021). Properties of wood–plastic composites manufactured from two differentwood feedstocks: Wood flour and wood pellets. *Polymers*, *13*(16). https://doi.org/10.3390/polym13162769

Zhang, H., Li, D., Huang, T., Hu, Q., Jiang, Q., & Wang, J. (2024). Investigation of a 3D Printing Method for Continuous Carbon Fiber-Reinforced Thermosetting Epoxy Composite. *Applied Composite Materials*, *31*(3), 911–928. https://doi.org/10.1007/s10443-024-10207-2

Yang, T. H., Leu, S. Y., Yang, T. H., & Lo, S. F. (2012). Optimized material composition to improve the physical and mechanical properties of extruded wood-plastic composites (WPCs). *Construction and Building Materials*, *29*, 120–127. https://doi.org/10.1016/j.conbuildmat.2011.09.013

Bansode, A., Barde, M., Asafu-Adjaye, O., Patil, V., Hinkle, J., Via, B. K., Adhikari, S., Adamczyk, A. J., Farag, R., Elder, T., Labbé, N., & Auad, M. L. (2021). Synthesis of Biobased Novolac Phenol-Formaldehyde Wood Adhesives from Biorefinery-Derived Lignocellulosic Biomass. *ACS Sustainable Chemistry and Engineering*, *9*(33), 10990–11002. https://doi.org/10.1021/acssuschemeng.1c01916

Gardner, D. J., & Wang, L. (n.d.). *ADDITIVE MANUFACTURING OF WOOD-BASED MATERIALS FOR COMPOSITE APPLICATIONS Background and Requirements*. https://www.slideshare.net/HorizonWatching/s12-3-d-printing-2014-

Hietala, M., Niinimäki, J., & Oksman, K. (2011). *The use of twin-screw extrusion in processing of wood: The effect of processing parameter and pretreatment*. BioResources, 6(4), 4615–4625. readpaper.com+2bioresources.cnr.ncsu.edu+2pmc.ncbi.nlm.nih.gov+2

Oksman, K., & Clemons, C. (1998). Mechanical properties and morphology of impact modified polypropylene-wood flour composites. *Journal of Applied Polymer Science*, *67*(9), 1503–1513. https://doi.org/10.1002/(SICI)1097-4628(19980228)67:9<1503::AID-APP1>3.0.CO;2-H

Ribeiro, L. S., Stolz, C. M., Amario, M., Silva, A. L. N. da, & Haddad, A. N. (2023). Use of Post-Consumer Plastics in the Production of Wood-Plastic Composites for Building Components: A Systematic Review. In *Energies* (Vol. 16, Issue 18). Multidisciplinary Digital Publishing Institute (MDPI). https://doi.org/10.3390/en16186549

Asafu-Adjaye, O. A., Street, J., Bensode, A., Auad, M. L., Peresin, M. S., Adhikari, S., Liles, T., & Via, B. K. (2022). Fast Pyrolysis Bio-Oil-Based Epoxy as an Adhesive in Oriented Strand Board Production. *Polymers*, *14*(6). https://doi.org/10.3390/polym14061244

El-Sayegh, S., Romdhane, L., & Manjikian, S. (2020). A critical review of 3D printing in construction: benefits, challenges, and risks. In *Archives of Civil and Mechanical Engineering* (Vol. 20, Issue 2). Springer. https://doi.org/10.1007/s43452-020-00038-w

Pan, Y., Zhang, Y., Zhang, D., & Song, Y. (2021). *3D printing in construction: state of the art and applications*. https://doi.org/10.1007/s00170-021-07213-0/Published

Saba N, Jawaid M, Alothman OY, Paridah M, Hassan A. Recent advances in epoxy resin, natural fiber-reinforced epoxy composites and their applications. *Journal of Reinforced Plastics and Composites*. 2015;35(6):447-470. doi:10.1177/0731684415618459

Zuo, Z., Gong, J., Huang, Y., Zhan, Y., Gong, M., & Zhang, L. (2019). Experimental research on transition from scale 3D printing to full-size printing in construction. *Construction and Building Materials*, *208*, 350–360. https://doi.org/10.1016/j.conbuildmat.2019.02.171

Wang, Q. C., Yu, S. N., Chen, Z. X., Weng, Y. W., Xue, J., & Liu, X. (2023). Promoting additive construction in fast-developing areas: An analysis of policies and stakeholder perspectives. *Developments in the Built Environment*, *16*. https://doi.org/10.1016/j.dibe.2023.100271

Shahzad, Q., Shen, J., Naseem, R., Yao, Y., Waqar, S., & Liu, W. (2021). Influence of phase change material on concrete behavior for construction 3D printing. *Construction and Building Materials*, *309*. https://doi.org/10.1016/j.conbuildmat.2021.125121

Costa, F. N., & Ribeiro, D. V. (2020). Reduction in CO2 emissions during production of cement, with partial replacement of traditional raw materials by civil construction waste (CCW). *Journal of Cleaner Production*, *276*. https://doi.org/10.1016/j.jclepro.2020.123302

Felipe Arbeláez Pérez, O., Senior Arrieta, V., Hernán Gómez Ospina, J., Herrera Herrera, S., Ferney Rodríguez Rojas, C., & María Santis Navarro, A. (2024). Carbon dioxide emissions from traditional and modified

concrete. A review. In *Environmental Development* (Vol. 52). Elsevier B.V. https://doi.org/10.1016/j.envdev.2024.101036

Benhelal, E., Zahedi, G., Shamsaei, E., & Bahadori, A. (2013). Global strategies and potentials to curb CO2 emissions in cement industry. In *Journal of Cleaner Production* (Vol. 51, pp. 142–161). Elsevier Ltd. https://doi.org/10.1016/j.jclepro.2012.10.049

Miller, S. A., John, V. M., Pacca, S. A., & Horvath, A. (2018). Carbon dioxide reduction potential in the global cement industry by 2050. *Cement and Concrete Research*, *114*, 115–124. https://doi.org/10.1016/j.cemconres.2017.08.026

Tay, Y. W. D., Panda, B., Paul, S. C., Noor Mohamed, N. A., Tan, M. J., & Leong, K. F. (2017). 3D printing trends in building and construction industry: a review. *Virtual and Physical Prototyping*, *12*(3), 261–276. https://doi.org/10.1080/17452759.2017.1326724

Krapež Tomec, D., & Kariž, M. (2022). Use of Wood in Additive Manufacturing: Review and Future Prospects. In *Polymers* (Vol. 14, Issue 6). MDPI. https://doi.org/10.3390/polym14061174

U.S. Environmental Protection Agency. (2018). Wood: Material-Specific Data. Facts and Figures about Materials, Waste and Recycling. Retrieved from https://www.epa.gov/facts-and-figures-about-materials-waste-and-recycling/wood-material-specific-data

Carne, R. H. R., Alade, A. A., Orji, B. O., Ibrahim, A., McDonald, A. G., & Maughan, M. R. (2023). A screw extrusion-based system for additive manufacturing of wood: Sodium silicate thermoset composites. *Advances in Mechanical Engineering*, *15*(11). https://doi.org/10.1177/16878132231210373/ASSET/279F82D7-FF5C-4F3A-9280-227A2D1D8EBC/ASSETS/IMAGES/LARGE/10.1177_16878132231210373-FIG9.JPG

Orji, B. O., Thie, C., Baker, K., Maughan, M. R., & McDonald, A. G. (2023). Wood fiber - sodium silicate mixtures for additive manufacturing of composite materials. *European Journal of Wood and Wood Products*, *81*(1), 45–58. https://doi.org/10.1007/S00107-022-01861-Z/METRICS

Dixit, N., & Jain, P. K. (2020). 3D printed carbon fiber reinforced thermoplastic composites: A review. *Materials Today: Proceedings*, *43*, 678–681. https://doi.org/10.1016/j.matpr.2020.12.609

Pop, M. A., Croitoru, C., Bedő, T., Geaman, V., Radomir, I., Coșnița, M., Zaharia, S. M., Chicoș, L. A., & Miloșan, I. (2019). Structural changes during 3D printing of bioderived and synthetic thermoplastic materials. *Journal of Applied Polymer Science*, *136*(17). https://doi.org/10.1002/app.47382

Yang, T. H., Leu, S. Y., Yang, T. H., & Lo, S. F. (2012). Optimized material composition to improve the physical and mechanical properties of extruded wood-plastic composites (WPCs). *Construction and Building Materials*, *29*, 120–127. https://doi.org/10.1016/j.conbuildmat.2011.09.013

Chapter 2

Comparative Study of Bleached and Lignin-Containing Cellulose Nanofibrils as Reinforcements in Epoxy Composites

2.1 Abstract

This comparative study explores the influence of incorporating cellulose nanofibrils (CNFs) obtained from bleached and lignin-containing cellulose pulp as reinforcements in an epoxy matrix. The research aims to identify optimal nanocellulose loading levels for improved mechanical properties of corresponding composites. Bleached CNF (BCNF) and lignin-containing CNF (LCNF) were introduced at different weight percentages (0.5, 0.75, and 1%) using high-energy mechanical mixing, and the composites were characterized through mechanical, morphological, chemical, and thermal analyses. The results indicated that BCNF exhibited superior performance compared to LCNF in improving the mechanical properties of the epoxy composites. Specifically, a 0.75% BCNF loading significantly enhanced the composite's toughness (41% increase) and elastic modulus (79% increase) while reducing brittleness, making the material stronger and more ductile. In contrast, LCNF composites displayed lower mechanical performance and reduced ductility. The interaction between BCNF and the epoxy matrix was more pronounced, as confirmed by QCM-D and FTIR analysis, suggesting better compatibility. Thermal analysis showed that both BCNF and LCNF reduced the thermal stability of the epoxy matrix, but LCNF, with lignin, provided some protection. Lignin's aromatic and antioxidant structure helped maintain thermal resistance, making LCNF composites at 1% loading thermally comparable to neat epoxy. However, higher BCNF loading (1%) led to decreased mechanical properties, likely due to nanocellulose aggregation. This research highlights the potential of optimizing nanocellulose content for tailored performance in bio-based composite materials.

Keywords: *Bleached CNF (BCNF); Cellulose nanofibers (CNFs); Epoxy composites; Lignin-containing CNF (LCNF).*

2.2 Introduction

Epoxy resins are thermosetting polymers widely used as polymeric matrices in composite applications. They exhibit outstanding properties such as adhesion, chemical resistance, mechanical strength, thermal stability, and low shrinkage after curing (Omrani et al., 2008). However, when crosslinked, they become rigid and often brittle, limiting their application (Ansari et al., 2014; Frihart, 2023). In recent years, studies have focused on reinforcing epoxy polymeric matrices with nanomaterials, particularly those that are more environmentally friendly and bio-based (Ilyas et al., 2024; Saikia et al., 2019). Bio-based nanomaterials merge nanotechnology benefits with renewable advantages of biodegradability, recyclability, and low production costs (Österberg et al., 2023).

Cellulose nanofibrils (CNF) are advanced bio-based materials used to enhance various polymers, including thermosets (Kumar et al., 2024; Kuyumcu et al., 2024; Yusuf et al., 2024). They are typically produced by mechanically disintegrating cellulose fibers via high-pressure homogenization, microfluidization, or grinding, often after chemical or enzymatic pretreatment to improve fibrillation (Nechyporchuk et al., 2016; Nobuta et al., 2016). CNFs consist of both crystalline and amorphous regions (Park & Park, 2024; Zhang et al., 2013). It is possible to tune the chemical composition of CNFs by using raw materials with different cellulose and lignin contents, as the mechanical process does not alter the chemical structure of the resulting nanofibrils (Iglesias et al., 2020). Thus, CNFs can be obtained from fully bleached or lignin-containing cellulose fibers, yielding bleached or lignin-containing cellulose nanofibrils (BCNF or LCNF, respectively). LCNF is an economically viable alternative, as it allows the use of unbleached fibers as a starting material while preserving lignin's functionality. The presence of residual lignin on the cellulose fibers influences the surface energy of the resulting fibrils, increasing their hydrophobic character (Liu et al., 2023; Rojo et al., 2015). The lignin in LCNFs also confers higher thermal stability due to its crosslinking, which creates strong interconnections between phenylpropane units,

improving resistance to high temperatures while also protecting the cellulose chains from degradation (Iglesias et al., 2023). In contrast, CNFs obtained from bleached (BCNF), pristine cellulose fibers exhibit a more hydrophilic character due to the large number of exposed –OH groups per surface area (Hassan et al., 2021; Zhang et al., 2023).

Polymer nanocomposites have attracted increasing scientific and industrial interest due to their ability to significantly improve mechanical properties, dimensional stability, and barrier performance with minimal filler content (Mondal, 2018). In particular, cellulose nanofibers (CNFs) have emerged as a promising reinforcement material because of their renewable origin and biodegradability (Saikia et al., 2019), offering a sustainable alternative that enhances material performance while promoting environmental responsibility (Reshmy et al., 2020). Previous studies have reported a significant improvement in the properties of epoxy composite materials when adding cellulose nanofibers (Neves et al., 2021). A study by Roszowska-Jarosz et al. (2021) demonstrated that BCNF incorporation significantly enhanced epoxy composites, with a 1% addition increasing tensile strength by 15% and 0.5% improving elongation at break by 102%. Saba et al. (2017) reported optimal tensile strength (26.7 MPa) at 0.75% BCNF, while higher loading (1%) led to decreased performance due to agglomeration. Similarly, Yusra et al. (2015) observed improved strength and modulus at 0.75%, but reduced elongation. Wongjaiyen et al. (2018) found that BCNF concentrations up to 3% improved tensile strength and Young's modulus, though higher levels limited ductility. These results suggest that moderate BCNF loading optimizes mechanical properties, while excessive content negatively affects composite performance.

The presence of residual lignin in LCNF can enhance fiber–matrix compatibility due to lignin's hydrophobic nature (Iglesias et al., 2020; Rojo et al., 2015). Although research on LCNF-reinforced epoxy systems is limited, available studies show promising results. Nair et al. (2017) observed that incorporating 20–36 wt% LCNF nearly doubled the tensile modulus and strength, with minimal impact on thermal stability. Similarly, Wang et al. (2020) reported that 1 wt% LCNF improved tensile strength by 81% and toughness by 185%, along with enhanced thermal resistance. Nonetheless, the specific influence of residual lignin on composite performance remains inadequately understood.

To address the knowledge gap regarding the role of residual lignin in cellulose nanofibrils (CNFs) on the performance of epoxy composites, this study systematically investigates the incorporation of bleached (BCNF) and lignin-containing CNFs (LCNF) into an epoxy matrix. The nanofibrils were added at varying weight fractions (0.5%, 0.75%, and 1%) and dispersed using high-energy mechanical mixing to ensure homogeneous distribution within the matrix. The nanocomposites were evaluated in terms of their mechanical and thermal properties imparted by BCNF and LCNF. A comprehensive set of characterizations was conducted, including mechanical testing to assess modulus and toughness, and morphological analysis to observe fiber dispersion and structure, using a universal testing machine and scanning electron microscopy (SEM), respectively, and chemical interaction evaluation through Fourier Transform Infrared Spectroscopy (FTIR) and Quartz Crystal Microbalance with Dissipation (QCM-D). Additionally, thermal analysis was performed to examine the impact of nanofiber content on the stability of the composites. This multifaceted approach provides a detailed comparison of the effects of lignin content and CNF loading, helping identify optimal reinforcement conditions for enhancing the performance of epoxy nanocomposites.

2.3 Materials and Methods

2.3.1 Materials

The softwood kraft pulp used in this study was sourced from a commercial mill located in Alabama. Both bleached and unbleached pulps were thoroughly washed and dispersed in deionized water to prepare a 2.0 wt.% suspension. Following the procedure described by Iglesias et al. (2021), the suspension was subjected to mechanical fibrillation using a Masuko Supermasscolloider MKZA-10-15J (Masuko Sangyo Co., Ltd., Japan) until a gel-like cellulose nanofibril dispersion was obtained. Based on typical specifications for this type of pulp, the unbleached material exhibits a Kappa number of ~28, while the bleached pulp reaches an ISO brightness of around 88%.

The epoxy resin used in this study was a diglycidyl ether of bisphenol A (4,4’-isopropylidenediphenol-epichlorohydrin copolymer, Epon 828), supplied by Hexion Inc., USA. This resin

contains two epoxide groups with an epoxide equivalent weight (EEW) ranging from 185 to 192 g/eq. Its viscosity and density at 25 °C are 110–150 P and 1.16 g/cm³, respectively. The curing agent employed was polyoxypropylene diamine (D-400), obtained from Everchem Specialty Chemicals, USA. D-400 has a viscosity of 0.22 P and a density of 0.972 g/cm³, both measured at 20 °C. It has an average molecular weight of 430 g/mol and an amine hydrogen equivalent of 4.41 meq/g.

2.3.2 BCNF/ LCNF Characterization

2.3.2.1 Atomic Force Microscopy

The morphology of cellulose nanofibrils (CNFs) was examined using an Anton Paar TOSCA 400 AFM (Graz, Austria) operating in tapping mode with a silicon cantilever. Image analysis was performed with Gwyddion software (v2.49, SourceForge). Samples were prepared following the protocol by Iglesias et al. (2021), which involved UV-ozone cleaning of silicon substrates for 30 minutes, treatment with 0.1 wt% polyethylenimine for 15 minutes, and spin coating 80 µL of 0.01 wt% CNF suspension at 3200 rpm for 1 minute. Prior to coating, CNF suspensions were sonicated in a cold bath (10 min, 20 kW, 25% amplitude) to promote delamination. The samples were then dried at 80 °C for 20 minutes and stored in a desiccator until analysis. Fibril width distributions were obtained from AFM images using ImageJ software, following a similar measurement approach described by Iglesias (2020). For each CNF, one hundred measurements were taken.

2.3.2.2 Fourier-transform infrared spectroscopy (FTIR)

The chemical composition of BCNF/LCNF samples was analyzed by Fourier-transform infrared spectroscopy (FTIR). Spectra were recorded in the range of 4000–450 cm^{-1} at room temperature using a PerkinElmer Spectrum 400 FTIR imaging system (PerkinElmer, USA).

2.3.2.3 Zeta Potential

The colloidal stability of the BCNF/LCNF suspensions was determined by measuring zeta potential using an Anton Paar Litesizer 500 (Graz, Austria). The zeta potential of the samples was analyzed through dynamic light scattering (DLS) using a Litesizer 500 (Anton Paar, Austria) with a dosing system. The samples were prepared at a 0.1 wt% concentration, adjusted to ~pH 7, and stirred magnetically for 10 minutes.

2.3.2.4 Interfacial Phenomena Studies

2.3.2.4.1 Quartz crystal microbalance with dissipation monitoring (QCM-D)

Interfacial interactions between Epon 828 and Jeffamine D-400 with BCNF and LCNF were investigated using a QSense QCM-D analyzer (Biolin Scientific, Västra Frölunda, Sweden). Model surfaces were prepared by spin coating BCNF or LCNF suspensions onto gold-coated quartz crystals, followed by stabilization in acetone to ensure complete surface conditioning. QCM-D measurements were performed by monitoring changes in frequency and dissipation of the quartz crystal, as described by Nypelö et al. (2012). Epon 828 and D-400 were individually introduced over the BCNF- or LCNF-coated sensors at a constant flow rate of 100 μL/min, and the resulting shifts in frequency and dissipation were recorded. The adsorption of these compounds led to the buildup of a soft film on the sensor surface, resulting in measurable dissipation effects. To accurately describe the viscoelastic behavior of the adsorbed layers, the Broadfit model implemented in the QSense DFind software was employed.

2.3.3 Fabrication and Characterization of Epoxy/CNF Nanocomposites

2.3.3.1 Production of Epoxy/CNF Nanocomposites

The freeze-dried cellulose nanofibers were added to D-400 at the weight percentages of 0.5, 0.75, and 1% relative to the epoxy resin. The mixture was stirred using a magnetic stirrer for 1 hour. Then, a homogenizer model T18 Ultraturrax was used at different speeds of 8 - 15 × 10^3 rpm to further disperse cellulose nanofibrils into the curing agent. Afterward, Epon 828 resin was added and mixed for 1 minute.

The weight ratio of Epon 828 to D-400 was 100:55. Finally, the mixture was poured into the mold, and the samples were allowed to cure for 24 hours at 35 °C in the oven. After this time, the post-curing process was carried out at 105 °C for 2 hours and finally at 120 °C for 1 hour. The same process was carried out to produce control composites without cellulose nanofibers. Five specimens were constructed for each nanomaterial loading level. A total of five baseline composites without nanomaterial and 30 composites enhanced with cellulose nanofibers were fabricated.

2.3.3.2 Tensile Properties

Tensile tests on the nanocomposites were conducted in accordance with ASTM D638 at a crosshead speed of 0.5 mm/min. For each composite formulation, five specimens with a thickness of 3.5 mm were tested. The toughness (strain energy at failure) was calculated as the area under the stress–strain curve up to the point of fracture.

2.3.3.3 Scanning Electron Microscopy (SEM)

After the tensile test, detailed examination of the fracture surfaces was carried out using a Zeiss EVO 50 Scanning Electron Microscope (SEM), equipped with ZEISS SmartSEM software (Carl Zeiss AG, Oberkochen, Germany). Prior to imaging, the samples were prepared using the EMS Q150R Sputter Coating Device, which facilitated the deposition of a thin gold coating on the fracture surfaces.

2.3.3.4 Fourier-transform infrared spectroscopy (FTIR)

Thereafter, the chemical composition of the samples was investigated using a Thermo Nicolet NEXUS 470 FTIR spectrometer (Thermo Fisher Scientific, USA), and for thermal characterization, the Thermogravimetric Analyzer (TGA) Q500 (TA Instruments, USA) was used. TGA analysis was conducted over a temperature range of 30–600 °C, with a heating rate of 20 °C/min under a nitrogen atmosphere.

2.4 Results and Discussion

2.4.1 Cellulose Nanofibrils (BCNF and LCNF) Properties

Figure 2.1 shows the AFM micrographs of the surface morphology and dimensions of BCNF and LCNF. The AFM image of the LCNF sample reveals a dense and entangled network of nanofibrils with varying diameters, indicating a heterogeneous structure (Correia et al., 2016). The average width of LCNFs was 0.059 ± 0.016 μm (range: 0.031–0.09 μm). This more complex topography is likely influenced by the presence of residual lignin, which promotes the formation of branched and interconnected fibril networks (Yuan et al., 2021). In contrast, the BCNF image displays a more uniform and individualized fibrillar structure, with thinner and more evenly distributed nanofibers. The average width of BCNFs was 0.052 ± 0.012 μm (range: 0.021–0.08 μm). These morphological differences highlight how chemical composition and processing conditions directly influence the nanofibril structure, particularly through the effect of lignin content.

Softwoods, the primary source of these fibers, typically contain 41–46% cellulose, 25–32% hemicellulose, and 26–31% lignin, with minor extractives (10–25%) and ash (0.2–0.4%) (Thomas, 1977; Gullichsen & Paulapuro, 1999). During pulping, lignin is mainly removed to liberate the cellulose fibers, and its residual content is monitored using the Kappa number, which indicates the degree of delignification and the pulp's bleachability (Segura et al., 2016). In industrial practice, softwood pulps are usually cooked to a Kappa number of 28–34 to achieve an optimal balance between lignin removal, pulp yield, and fiber strength (Shackford, 2003). For instance, unbleached softwood pulp may have a Kappa number of around 26.8 (equivalent to ~4% lignin content), which can be reduced to about 3.2 (~0.5% lignin) through bleaching (Popescu et al., 2008).

However, not all contributions to the Kappa number come from residual lignin alone. Hexenuronic acids (HexA), formed from xylan hemicelluloses during alkaline pulping, also contribute approximately 1–3 Kappa units (Jiang et al., 2002). Typically, about 11.6 mmol of HexA corresponds to one Kappa unit (Burkhardt, 2018; Popescu et al., 2008; Brogdon, 2009). HexA formation occurs rapidly during cooking,

beginning early in the pulping process, and its degradation is an important factor influencing final pulp properties (Sixta & Rutkowska, 2006).

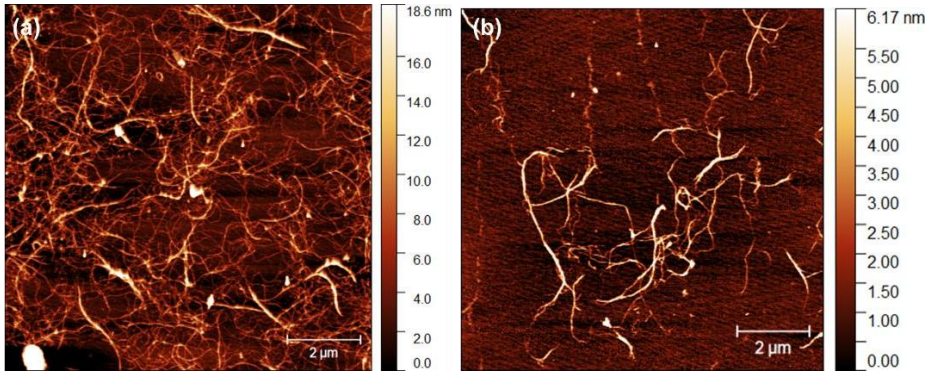

Fig. 2.1 AFM height micrographs of LCNF (a) and BCNF (b)

FTIR spectra and zeta potential data are presented in **Figures 2.2a** and **2.2b**, respectively, providing insight into the chemical structure and colloidal stability of the neat BCNF and LCNF used in the nanocomposites. Both spectra show a broad absorption band at around 3330 cm^{-1}, corresponding to hydroxyl (O–H) stretching vibrations typical of cellulose crystalline regions. This peak appears slightly more intense in BCNF, consistent with its higher crystallinity (Mamat Razali et al., 2021; Roszowska-Jarosz et al., 2021). Peaks near 2900 cm^{-1}, attributed to alkyl (C–H) stretching, are observed in both samples (Aema et al., 2017). A peak at approximately 1600 cm^{-1} is observed in both BCNF and LCNF samples, which can be attributed to aromatic skeletal vibrations from the benzene rings of lignin (Morán et al., 2008). The spectral similarities between neat LCNF and BCNF suggest that traces of residual lignin may still be present in the bleached nanocellulose (BCNF) (Baraka et al., 2023; Lani et al., 2014).

The zeta potential results (**Figure 2.2b**) show that BCNF has slightly higher colloidal stability compared to LCNF, which may be attributed to the presence of additional carboxyl and hydroxyl groups present in lignin that contribute to greater surface charge (Liu et al., 2023). According to Herrera et al. (2018), suspensions with zeta potentials above +30 mV or below –30 mV are considered stable. Moreover, the magnitude of zeta potential can be indicative of the surface functional groups, particularly the concentration of carboxyl groups (Liu et al., 2023; Xu et al., 2021).

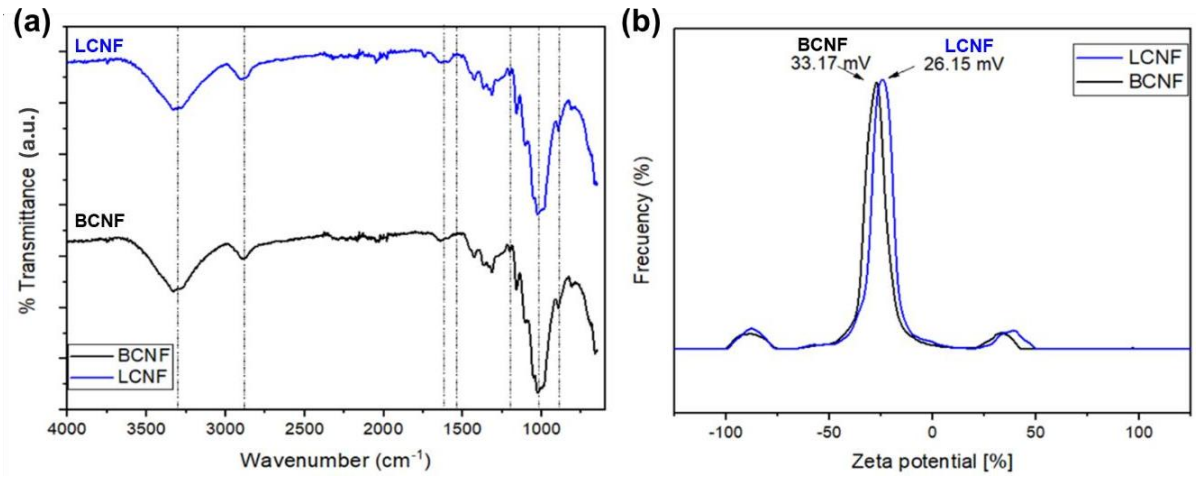

Fig. 2.2 (a) Fourier-transform infrared (FTIR) spectra comparing BCNF and LCNF; (b) Zeta potential characterization of BCNF and LCNF suspensions at pH ~7

2.4.2 Interfacial Interaction in Cellulose Nanofibril–Resin System

Figure 2.3 presents the QCM-D analysis of BCNF- and LCNF-coated gold sensors upon exposure to D-400 and epoxy resins. Both CNF types exhibited a more significant frequency decrease (Δf) and increased dissipation (ΔD) when D-400 was introduced, compared to epoxy. This indicates a greater mass uptake and the formation of a more viscoelastic layer with D-400, suggesting stronger interactions between D-400 and the CNF surfaces, more so in the case of BCNF, which can be attributed to hydrophilic interactions facilitated by polar interaction and favorable hydrogen bonding (Villada· et al., 2021). D-400, a polyetheramine, contains multiple ether and amine groups, enhancing its hydrophilicity, leading to increased adsorption and a more hydrated interfacial layer. In contrast, epoxy resins like Epon 828 are more hydrophobic, resulting in weaker interactions with the hydrophilic CNFs and thus lower mass uptake and dissipation changes. Based on these observations, D-400 was selected for initial mixing with BCNF or

LCNF to produce the nanocomposites, leveraging the strong interfacial interactions. Subsequently, epoxy was added to the matrix to enhance the mechanical properties of the final composite material.

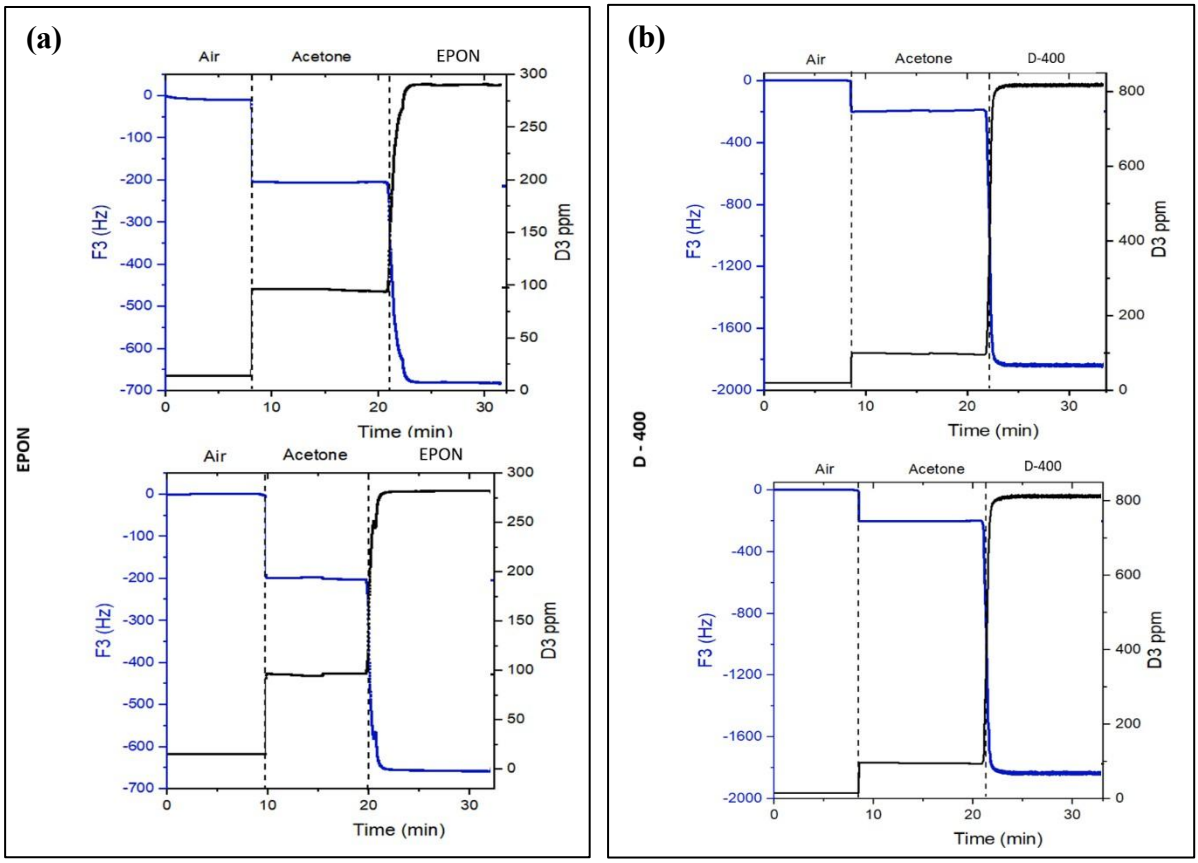

Fig. 2.3 QCM-D interaction profiles of (a) epoxy resin and (b) D-400 with BCNF (top) and LCNF (bottom) coated surfaces

2.4.3 Performance of Epoxy/CNF Nanocomposites

2.4.3.1 Mechanical properties

Mechanical performance was further evaluated by determining the elastic modulus and toughness of nanocomposites reinforced with BCNF and LCNF at 0, 0.5, 0.75, and 1 wt% loadings, as shown in **Figure 2.4**. Nanocomposites containing 0.75 wt% and 1 wt% BCNF exhibited significant improvements in both toughness (41% and 10%, respectively) and elastic modulus (79% and 58%, respectively) compared

to the neat epoxy composite. The 0.75 wt% BCNF formulation notably enhanced the composite's mechanical behavior, reducing brittleness by increasing both stiffness and energy absorption capacity before failure. In contrast, LCNF-reinforced composites exhibited lower toughness, reduced overall mechanical performance, and limited deformability compared to both the neat epoxy and the BCNF-reinforced composites. This inferior behavior may be attributed to the higher amorphous content and lower cellulose fraction in LCNF. While cellulose contributes to greater stiffness and strength, hemicellulose and lignin—more abundant in LCNF—are typically associated with increased deformability and lower mechanical integrity (Aema et al., 2017; Mamat Razali et al., 2021). Beyond the intrinsic properties of the nanofibers and the epoxy matrix, interfacial compatibility also plays a critical role in mechanical performance. Based on QCM-D data, BCNF showed stronger interactions with the epoxy system than LCNF, supporting the observed differences in reinforcement efficiency. However, at 1 wt% BCNF, performance declined—likely due to nanofiber agglomeration and poor dispersion, which hinder effective stress transfer. This trend is consistent with previous findings reported by Saba et al. (2017) and Lanna et al. (2020).

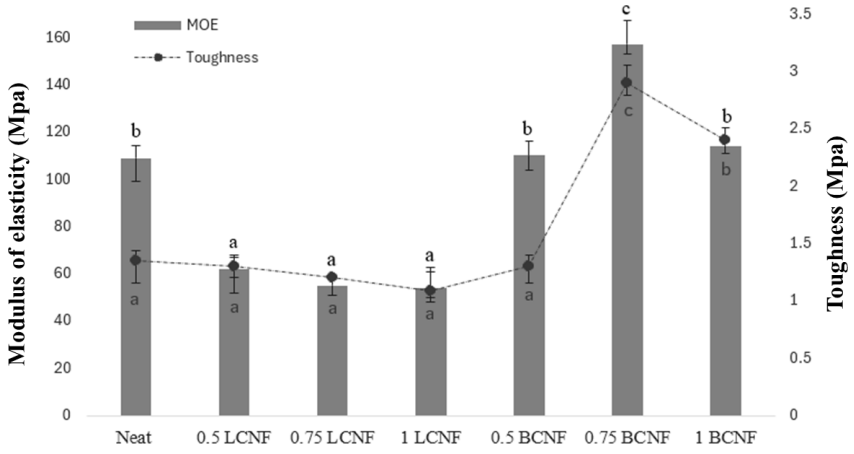

Fig. 2.4 Elastic modulus and toughness for nanocomposites with BCNF and LCNF at different loading percentages (0, 0.5, 0.75, and 1%)

2.4.3.2 Morphological properties

To further understand the mechanical performance of the nanocomposites, scanning electron microscopy (SEM) was used to examine the fracture surfaces after tensile testing. As shown in **Figure 2.5a**, the fracture surface of the neat epoxy exhibits a smooth texture, indicative of its brittle nature and limited resistance to crack propagation, attributed to its high cross-linking density (Lin et al., 2018; Shrestha et al., 2019). Conversely, in the composites with cellulose nanofibrils (BCNF/LCNF), the fracture surface became significantly rougher. This is because nanocellulose, serving as a reinforcing material, enables stress distribution, thereby facilitating the formation of cracks (Gabr et al., 2014). The composite with a 0.75% loading of BCNF (**Figure 2.5b**) shows a more uniform distribution within the matrix compared to the 1% loading. In the latter case (**Figure 2.5c**), the aggregation of cellulose nanofibrils caused stress concentration points, which had adverse effects on the properties of the nanocomposites (Hu et al., 2021). This phenomenon could explain why nanocellulose with 0.75% loading exhibits improved mechanical properties compared to the nanocomposite with 1% loading. Although the composites with LCNF exhibited a rougher fracture surface compared to the neat epoxy, the presence of air bubbles may have reduced the mechanical properties of LCNF (**Figure 2.5d**).

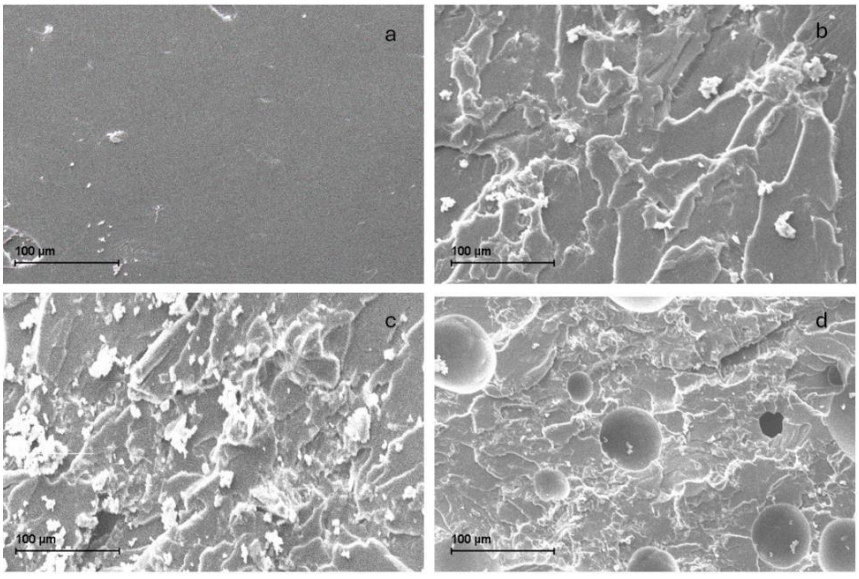

Fig. 2.5 Fracture morphology of the composite post-tensile testing: (a) Neat Epoxy, (b) Epoxy/0.75% BCNF, (c) Epoxy/1% BCNF and (d) Epoxy/0.75% LCN

2.4.3.3 Nanocomposites chemical analysis

Figure 2.6 shows the FTIR spectra of the nanocomposites to investigate the characteristic functional groups and assess chemical interactions in the nanocomposite systems. In the spectra of neat LCNF and BCNF, a peak at 3330 cm^{-1} is observed, corresponding to the hydroxyl (O-H) group associated with the crystalline domains of cellulose in nanocellulose (higher in BCNF) (Mamat Razali et al., 2021; Roszowska-Jarosz et al., 2021). Additionally, in CNF-Reinforced epoxy nanocomposites, the hydroxyl peak shifts to ~3400 cm^{-1} and gradually decreases as the nanocellulose content increases. This shift suggests the formation of hydrogen bonds between both CNFs and the epoxy matrix, likely due to OH interactions between the resin and the nanocellulose (Yue et al., 2021).

In the nanocomposite material (Epoxy/CNF), the range from 2981.4 to 2798.2 cm^{-1} corresponds to the broad vibrations of aliphatic CH_2 and CH_3 groups, attributed to the presence of the amine hardener and epoxy resin (Saba et al., 2017; Xu et al., 2013). In the nanocomposites, the band at ~1640 cm^{-1} is likely due to the overlap between the C=C stretching of the epoxide group and the -NH_2 scissoring of the amine group (Aema et al., 2017; González et al., 2012; Saba et al., 2017). The peak at 1032 cm^{-1} is attributed to the C–O stretching in ether linkages, while the peak around 920 cm^{-1}, corresponding to oxirane ring vibrations, likely indicates the presence of unreacted epoxy groups (Saba et al., 2017; Xu et al., 2013). In Epoxy/CNF composites, epoxide groups can react with amine (NH_2) or CNF hydroxyl groups, leading to the formation of ether and hydroxyl groups (Xu et al., 2013). Since their absorption bands overlap in the 1000–1250 cm^{-1} range, FTIR alone cannot confirm the role of CNFs as chain extenders or crosslinkers. However, the decrease in intensity of the 912 cm^{-1} peak suggests a greater extent of epoxide group reaction (Xu et al., 2013). As the nanocellulose content increases, the intensities of these peaks diminish, implying stronger interactions between the epoxy groups and the nanocellulose. Similarly, the peak at 828 cm^{-1} is associated with C–O–C stretching vibrations of the oxirane group. In BCNF composites, the intensity of this peak is lower, suggesting a reduction in the concentration of unreacted oxirane groups, which confirms interactions between the epoxy matrix and nanocellulose fibers (Parames et al., 2021).

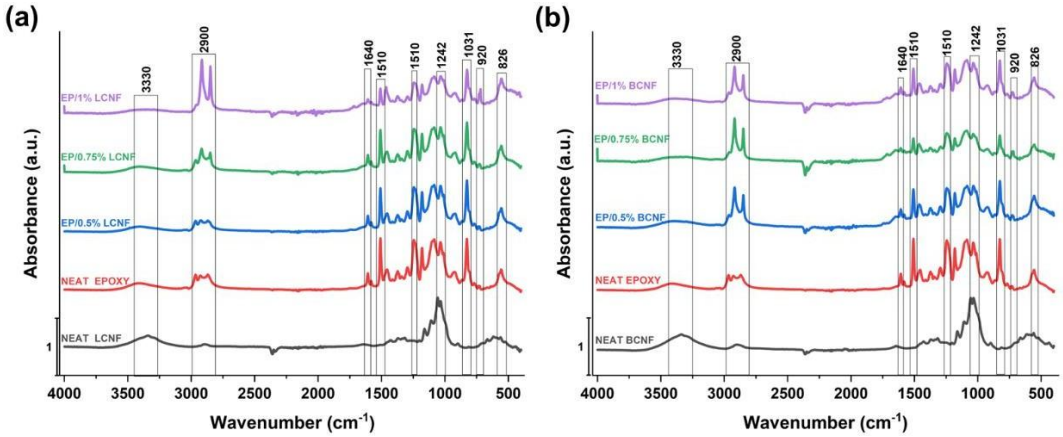

Fig. 2.6 FTIR spectrum for the nanocomposites with BCNF (a) and LCNF (b)

2.4.3.4 Thermal properties

The thermal stability of the nanocomposites with different percentages of BCNF and LCNF was investigated using TGA, aiming at evaluating their thermal stability (**Figure 2.7**). Neat nanocellulose samples, both lignin-containing and bleached, degrade more rapidly than their composite counterparts. Hemicellulose decomposes in the range of 180-340 °C, which is lower than cellulose, which decomposes between 230-450 °C (Flores et al., 2020), while the degradation events occurring at higher temperatures are attributed to the oxidation of the remaining organic matter (Gracia-Fernández et al., 2005). It can be observed that the epoxy matrix is a highly thermally stable material (**Figures 2.7a** and **2.7b**), and adding nanocellulose decreases stability, the same findings by Raghavendra et al. (2014). Since the thermal decomposition of cellulose-based materials occurs at lower temperature ranges, nanocellulose can introduce functional groups that are more susceptible to thermal decomposition, resulting in a decrease in the thermal stability of the epoxy matrix (Aema et al., 2017).

In the case of the nanocomposites with LCNF (**Figure 2.7a**), as the percentage of nanocellulose increases, the composites require more thermal energy to degrade, but not as high as neat epoxy. This behavior is more evident in the derivative curves of LCNF, where a small curve appears around the range of 440-500 °C, indicating the oxidation process of lignin (Ramiah, 1970). Although the analysis was

conducted in a nitrogen environment, it is possible that small traces of oxygen were present due to residual oxygen in the system or oxygen adsorbed onto the lignin surface, allowing for partial oxidation to occur under these conditions. On the other hand, in the BCNF graphs (**Figure 2.7b**), it can be observed that the opposite process occurs; as nanocellulose increases, especially in 0.75% of LCNF, less thermal energy is required to degrade the compound since lignin can protect cellulose from early decomposition (Sabaruddin et al., 2021). However, other groups have reported that by incorporating bleached nanocellulose, the thermal degradation of the epoxy composite is lower compared to neat epoxy (Aema et al., 2017; Sun et al., 2022).

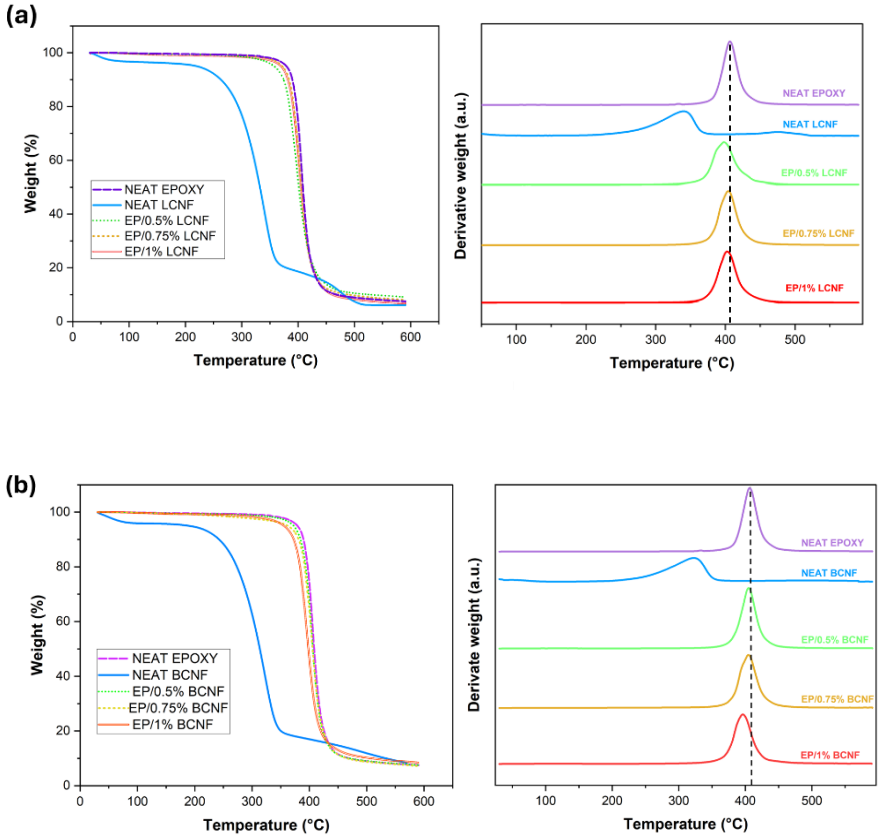

Fig. 2.7 Thermogravimetric analysis (TGA) and derivative thermogravimetric (DTG) curves of nanocomposites reinforced with LCNF (a) and BCNF (b)

2.5 Conclusions

This study demonstrated that incorporating BCNF and LCNF into epoxy composites significantly influenced their mechanical and thermal properties. BCNF outperformed LCNF in enhancing mechanical performance but did not improve thermal stability. A 0.75% BCNF loading enhanced both stiffness and ductility, making the composite tougher and more energy-absorbing, while 1% BCNF loading led to decreased performance due to aggregation and stress concentration. FTIR and QCM-D results suggest improved compatibility and interaction of BCNF with the epoxy matrix compared to LCNF. Thermal analysis revealed that nanocellulose decreased the overall thermal stability of the epoxy matrix; the presence of lignin in LCNF offered some protective effects at higher temperatures. Despite this, nanocellulose's susceptibility to thermal degradation contributed to reduced thermal stability in the nanocomposites.

2.6 References

Aema, I., Ma, W., Shafaamri, A., Kasi, R., Zaini, F. N., Balakrishnan, V., Subramaniam, R., & Arof, A. K. (2017). Epoxy/nanocellulose coating. In *BioResources* (Vol. 12, Issue 2). https://bioresources.cnr.ncsu.edu/resources/anticorrosion-properties-of-epoxynanocellulose-nanocomposite-coating/

Ansari, F., Galland, S., Johansson, M., Plummer, C. J. G., & Berglund, L. A. (2014). Cellulose nanofiber network for moisture stable, strong and ductile biocomposites and increased epoxy curing rate. *Composites Part A: Applied Science and Manufacturing*, *63*, 35–44. https://doi.org/10.1016/j.compositesa.2014.03.017

Baraka, F., Robles, E., & Labidi, J. (2023). Microwave-assisted esterification of bleached and unbleached cellulose nanofibers. *Industrial Crops and Products*, *191*. https://doi.org/10.1016/j.indcrop.2022.115970

Brogdon, B. N. (2009). A FUNDAMENTAL REVIEW AND CRITICAL ANALYSIS OF HEXENURONIC ACIDS AND THEIR IMPACT IN ELEMENTAL CHLORINE-FREE BLEACHING. TAPPI Engineering, Pulping & Environmental Conference (Memphis, TN USA; Oct. 11-14, 2009)

Burkhardt, S. (2018). Does the kappa number method accurately reflect lignin content in nonwood pulps? *Tappi Journal*, *17*(11), 611–617. https://doi.org/10.32964/TJ17.11.611

Correia, V. da C., dos Santos, V., Sain, M., Santos, S. F., Leão, A. L., & Savastano Junior, H. (2016). Grinding process for the production of nanofibrillated cellulose based on unbleached and bleached bamboo organosolv pulp. Cellulose, 23(5), 2971–2987. https://doi.org/10.1007/s10570-016-0996-9

Flores, J. J. A., Quiñones, J. G. R., Rodríguez, M. L. Á., Vera, J. V. A., Valencia, J. E., Martínez, S. J. G., Montesino, F. M., & Rosas, A. A. (2020). Thermal degradation kinetics and FT-IR analysis on the pyrolysis of pinus pseudostrobus, pinus leiophylla and pinus montezumae as forest waste in western Mexico. *Energies*, *13*(4). https://doi.org/10.3390/en13040969

Frihart, C. R. (2023). Epoxy adhesives from natural materials. In *Biobased Adhesives: Sources, Characteristics, and Applications* (pp. 367–393). wiley. https://doi.org/10.1002/9781394175406.ch12

Gabr, M. H., Phong, N. T., Okubo, K., Uzawa, K., Kimpara, I., & Fujii, T. (2014). Thermal and mechanical properties of electrospun nano-celullose reinforced epoxy nanocomposites. *Polymer Testing*, *37*, 51–58. https://doi.org/10.1016/j.polymertesting.2014.04.010

González, M. G., Cabanelas, J. C., & Baselga, J. (2012). Applications of FTIR on Epoxy Resins - Identification, Monitoring the Curing Process, Phase Separation and Water Uptake. In *Infrared Spectroscopy - Materials Science, Engineering and Technology*. InTech. https://doi.org/10.5772/36323

Gracia-Fernández, C. A., Gómez-Barreiro, S., Ruíz-Salvador, S., & Blaine, R. (2005). Study of the degradation of a thermoset system using TGA and modulated TGA. *Progress in Organic Coatings*, *54*(4), 332–336. https://doi.org/10.1016/j.porgcoat.2005.08.002

Gullichsen, J., & Fogelholm, C. (Eds.). (1999). *Chemical pulping* (Vol. 5). Atlanta, GA: TAPPI Press.

Hassan, M. L., Abou-Elseoud, W. S., Abdel Kader, A. H., & Hassan, E. A. (2021). Rice straw paper sheets reinforced with bleached or unbleached nanofibers. *Nordic Pulp and Paper Research Journal*, *36*(1), 139–148. https://doi.org/10.1515/npprj-2020-0073

Herrera, M., Thitiwutthisakul, K., Yang, X. *et al.* Preparation and evaluation of high-lignin content cellulose nanofibrils from eucalyptus pulp. *Cellulose* **25**, 3121–3133 (2018). https://doi.org/10.1007/s10570-018-1764-9

Hu, J., Kong, Z., Liu, K., Qin, J., Tao, Y., Zhou, L., Yuan, Y., Jiang, M., Duan, Y., & Zhang, J. (2021). Carboxylation of Cellulose Nanocrystals for Reinforcing and Toughing Rubber through Dual Cross-linking Networks. *ACS Applied Polymer Materials*, *3*(12), 6120–6129. https://doi.org/10.1021/acsapm.1c00975

Iglesias MC, Gomez-Maldonado D, Via BK et al (2020) Pulping processes and their effects on cellulose fibers and nanofibrillated cellulose properties: a review. For Prod J 70:10–21. https://doi.org/10.13073/FPJ-D-19-00038

Iglesias, M. C., Gomez-Maldonado, D., Davis, V. A., & Peresin, M. S. (2023). A review on lignocellulose chemistry, nanostructure, and their impact on interfacial interactions for sustainable products development. In *Journal of Materials Science* (Vol. 58, Issue 2, pp. 685–706). Springer. https://doi.org/10.1007/s10853-022-07992-1

Iglesias, M. C., Hamade, F., Aksoy, B., Jiang, Z., Davis, V. A., & Peresin, M. S. (2021). Correlations between rheological behavior and intrinsic properties of nanofibrillated cellulose from wood and soybean hulls with varying lignin content. *BioResources, 16*(3), 4831–4845

Iglesias, M. C., Shivyari, N., Norris, A., Martin-Sampedro, R., Eugenio, M. E., Lahtinen, P., … Peresin, M. S. (2020). The effect of residual lignin on the rheological properties of cellulose nanofibril suspensions. *Journal of Wood Chemistry and Technology*, *40*(6), 370–381. https://doi.org/10.1080/02773813.2020.1828472

Ilyas, R. A., Asyraf, M. R. M., Rajeshkumar, L., Awais, H., Siddique, A., Shaker, K., Nawab, Y., & Wahit, M. U. (2024). A review of bio-based nanocellulose epoxy composites. In *Journal of Environmental Chemical Engineering* (Vol. 12, Issue 5). Elsevier Ltd. https://doi.org/10.1016/j.jece.2024.113835

Jiang, Z.-H., van Lierop, B., & Berry, R. (2002). *Os ácidos hexenurônicos na química de papel e celulose* [Hexenuronic acids in pulp and paper chemistry] (Paprican Report). Pointe-Claire, QC, Canada: Paprican. Retrieved from https://www.eucalyptus.com.br/artigos/2002_HexsAcds_Chemistry.pdf

Kumar, B., Adil, S., Pham, D. H., & Kim, J. (2024). Environment-friendly, high-performance cellulose nanofiber-vanillin epoxy nanocomposite with excellent mechanical, thermal insulation and UV shielding properties. *Heliyon*, *10*(3). https://doi.org/10.1016/j.heliyon.2024.e25272

Kuyumcu, M., Kurtulus, C., Ciftci, M., & Tasdelen, M. A. (2024). Improving the mechanical properties of fiber-reinforced polymer composites through nanocellulose-modified epoxy matrix. *Express Polymer Letters*, *18*(1), 61–71. https://doi.org/10.3144/expresspolymlett.2024.5

Lani, N. S., Ngadi, N., Johari, A., & Jusoh, M. (2014). Isolation, characterization, and application of nanocellulose from oil palm empty fruit bunch fiber as nanocomposites. *Journal of Nanomaterials*, *2014*. https://doi.org/10.1155/2014/702538

Lanna, A., Suklueng, M., Kasagepongsan, C., & Suchat, S. (2020). Performance of Novel Engineered Materials from Epoxy Resin with Modified Epoxidized Natural Rubber and Nanocellulose or Nanosilica. *Advances in Polymer Technology*, *2020*. https://doi.org/10.1155/2020/2123836

Lin, J., Patterson, B. A., Malakooti, M. H., & Sodano, H. A. (2018). *Isolation of Aramid nanofibers for high strength multiscale fiber reinforced composites*. 52. https://doi.org/10.1117/12.2300515

Lin, S.Y. and Dence, C.W., Eds. (1992) Methods in Lignin Chemistry. Springer Series in Wood Science. Springer, Berlin, Heidelberg, 527-548. https://doi.org/10.1007/978-3-642-74065-7

Liu, Y., Zhang, S., Li, L., & Coseri, S. (2023). Cellulose nanofiber extraction from unbleached kraft pulp for paper strengthening. *Cellulose*, *30*(5), 3219–3235. https://doi.org/10.1007/s10570-022-05008-4

Mamat Razali, N. A., Ismail, M. F., & Abdul Aziz, F. (2021). Characterization of nanocellulose from Indica rice straw as reinforcing agent in epoxy-based nanocomposites. *Polymer Engineering and Science*, *61*(5), 1594–1606. https://doi.org/10.1002/pen.25683

Mondal, S. (2018). Review on Nanocellulose Polymer Nanocomposites. In *Polymer - Plastics Technology and Engineering* (Vol. 57, Issue 13, pp. 1377–1391). Taylor and Francis Inc. https://doi.org/10.1080/03602559.2017.1381253

Morán, J. I., Alvarez, V. A., Cyras, V. P., & Vázquez, A. (2008). Extraction of cellulose and preparation of nanocellulose from sisal fibers. *Cellulose*, *15*(1), 149–159. https://doi.org/10.1007/s10570-007-9145-9

Nair, S. S., Kuo, P.-Y., Chen, H., & Yan, N**.** (2017). Investigating the effect of lignin on the mechanical, thermal, and barrier properties of cellulose nanofibril reinforced epoxy composite. *Industrial Crops and Products, 100*, 208–217. https://doi.org/10.1016/j.indcrop.2017.02.032

Nechyporchuk, O., Belgacem, M. N., & Bras, J. (2016). Production of cellulose nanofibrils: A review of recent advances. In *Industrial Crops and Products* (Vol. 93, pp. 2–25). Elsevier B.V. https://doi.org/10.1016/j.indcrop.2016.02.016

Neves, R. M., Ornaghi, H. L., Zattera, A. J., & Amico, S. C. (2021). Recent studies on modified cellulose/nanocellulose epoxy composites: A systematic review. In *Carbohydrate Polymers* (Vol. 255). Elsevier Ltd. https://doi.org/10.1016/j.carbpol.2020.117366

Nobuta, K., Teramura, H., Ito, H., Hongo, C., Kawaguchi, H., Ogino, C., Kondo, A., & Nishino, T. (2016). Characterization of cellulose nanofiber sheets from different refining processes. *Cellulose*, *23*(1), 403–414. https://doi.org/10.1007/s10570-015-0792-y

Nypelö, T., Pynnönen, H., Österberg, M., Paltakari, J., & Laine, J. (2012). Interactions between inorganic nanoparticles and cellulose nanofibrils. *Cellulose*, *19*(3), 779–792. https://doi.org/10.1007/s10570-012-9656-x

Omrani, A., Simon, L. C., & Rostami, A. A. (2008). Influences of cellulose nanofiber on the epoxy network formation. *Materials Science and Engineering: A*, *490*(1–2), 131–137. https://doi.org/10.1016/j.msea.2008.01.012

Österberg, M., Henn, K. A., Farooq, M., & Valle-Delgado, J. J. (2023). Biobased Nanomaterials─The Role of Interfacial Interactions for Advanced Materials. In *Chemical Reviews* (Vol. 123, Issue 5, pp. 2200–2241). American Chemical Society. https://doi.org/10.1021/acs.chemrev.2c00492

Parameswaranpillai, Jyotishkumar., Pulikkalparambil, Herikrishnan., Rangappa, S. Mavinkere., & Siengchin, Suchart. (2021). *Epoxy composites preparation, characterization and applications*. Wiley-VCH.

Park, W. H., & Park, J. S. (2024). Exploring the Relative Degree of Crystalline and Amorphous Properties of Cellulose Nanofibrils Studied by Correlated Graphene-Quenching Raman Spectroscopy with Electrostatic Force Microscopy Technique. *Journal of the Korean Chemical Society*, *68*(6), 335–342. https://doi.org/10.5012/jkcs.2024.68.6.335

Popescu, C.-M., Tibirna, C. M., Raschip, I. E., Popescu, M.-C., Ander, P., & Vasile, C. (2008). BULK AND SURFACE CHARACTERIZATION OF UNBLEACHED AND BLEACHED SOFTWOOD KRAFT PULP FIBRES. In *CELLULOSE CHEMISTRY AND TECHNOLOGY Cellulose Chem. Technol* (Vol. 42, Issue 9).

Raghavendra, G., Ojha, S., Acharya, S. K., & Pal, S. K. (2014). Jute fiber reinforced epoxy composites and comparison with the glass and neat epoxy composites. *Journal of Composite Materials*, *48*(20), 2537–2547. https://doi.org/10.1177/0021998313499955

Ramiah, M. V. (1970). Thermogravimetric and differential thermal analysis of cellulose, hemicellulose, and lignin. *Journal of Applied Polymer Science*, *14*(5), 1323–1337. https://doi.org/10.1002/app.1970.070140518

Reshmy, R., Philip, E., Paul, S. A., Madhavan, A., Sindhu, R., Binod, P., Pandey, A., & Sirohi, R. (2020). Nanocellulose-based products for sustainable applications-recent trends and possibilities. In *Reviews in Environmental Science and Biotechnology* (Vol. 19, Issue 4, pp. 779–806). Springer Science and Business Media B.V. https://doi.org/10.1007/s11157-020-09551-z

Rojo, E., Peresin, M. S., Sampson, W. W., Hoeger, I. C., Vartiainen, J., Laine, J., & Rojas, O. J. (2015). Comprehensive elucidation of the effect of residual lignin on the physical, barrier, mechanical and surface properties of nanocellulose films. *Green Chemistry*, *17*(3), 1853–1866. https://doi.org/10.1039/c4gc02398f

Roszowska-Jarosz, M., Masiewicz, J., Kostrzewa, M., Kucharczyk, W., Żurowski, W., Kucińska-Lipka, J., & Przybyłek, P. (2021). Mechanical properties of bio-composites based on epoxy resin and nanocellulose fibres. *Materials*, *14*(13). https://doi.org/10.3390/ma14133576

Saba, N., Mohammad, F., Pervaiz, M., Jawaid, M., Alothman, O. Y., & Sain, M. (2017). Mechanical, morphological and structural properties of cellulose nanofibers reinforced epoxy composites. *International Journal of Biological Macromolecules*, *97*, 190–200. https://doi.org/10.1016/j.ijbiomac.2017.01.029

Sabaruddin, F. A., Tahir, P. M., Sapuan, S. M., Ilyas, R. A., Lee, S. H., Abdan, K., Mazlan, N., Roseley, A. S. M., & Khalil Hps, A. (2021). The effects of unbleached and bleached nanocellulose on the thermal and flammability of polypropylene-reinforced kenaf core hybrid polymer bionanocomposites. *Polymers*, *13*(1), 1–19. https://doi.org/10.3390/polym13010116

Saikia, A., Debbarma, N., & Karak, N. (2019). Renewable resource based hyperbranched epoxy thermosetting nanocomposite with cellulose nanofiber as a sustainable material. *Cellulose*, *26*(8), 4743–4755. https://doi.org/10.1007/s10570-019-02443-8

Segura, T. E. S., dos Santos, J. R. S., Sarto, C., & da Silva, J. F. G. (2016). Effect of Kappa Number Variation on Modified Pulping of Eucalyptus. *BioResources*, *11*(4), 9842–9855. https://doi.org/10.15376/BIORES.11.4.9842-9855

Shackford, L. D. (2003, October 13–16). *A comparison of pulping and bleaching of kraft softwood and eucalyptus pulps*. Paper presented at the International Pulp and Paper Congress and Exhibition, São Paulo, Brazil. Retrieved from https://www.celso-

foelkel.com.br/artigos/outros/A%20Comparison%20of%20Pulping%20and%20Bleaching%20of%20Kraft%20Softwood%20and%20Eucalyptus%20Pulps.pdf

Shrestha, S., Chowdhury, R. A., Toomey, M. D., Betancourt, D., Montes, F., & Youngblood, J. P. (2019). Surface hydrophobization of TEMPO-oxidized cellulose nanofibrils (CNFs) using a facile, aqueous modification process and its effect on properties of epoxy nanocomposites. *Cellulose*, *26*(18), 9631–9643. https://doi.org/10.1007/s10570-019-02762-w

Sixta, H., & Rutkowska, E. W. (2006). Comprehensive kinetic study of delignification, carbohydrate degradation, cellulose chain scissions, and hexenuronic acid reactions during kraft pulping of *Eucalyptus globulus*. *Lenzinger Berichte*, 86, 32–45.

Sun, J., Bai, J., & Li, J. (2022). The Synergistic Toughening and Strengthening Effects of Cork Particles and Nanocellulose on Rosin-Based Epoxy Resin. *Polymers*, *14*(23). https://doi.org/10.3390/polym14235064

Thomas, R. J. (1977). Wood: Structure and chemical composition. In L. I. Krall (Ed.), *Phenolic resins: A century of progress* (ACS Symposium Series No. 43, pp. 1–26). American Chemical Society. https://doi.org/10.1021/bk-1977-0043.ch001

Villada·, Y., Iglesias·, M. C., Olivares, M. L., Casis·, N., Zhu, J., Peresin, M. S., Estenoz, D., Iglesias, M. C., Peresin, · M S, & Zhu, J. (2021). Di-carboxylic acid cellulose nanofibril (DCA-CNF) as an additive in water-based drilling fluids (WBMs) applied to shale formations. *Cellulose*, *28*, 417–436. https://doi.org/10.1007/sl

Wang, Z., Gnanasekar, P., Sudhakaran Nair, S., Farnood, R., Yi, S., & Yan, N. (2020). Biobased Epoxy Synthesized from a Vanillin Derivative and Its Reinforcement Using Lignin-Containing Cellulose Nanofibrils. *ACS Sustainable Chemistry and Engineering*, *8*(30), 11215–11223. https://doi.org/10.1021/acssuschemeng.0c02559

Wongjaiyen, T., Brostow, W., & Chonkaew, W. (2018). Tensile properties and wear resistance of epoxy nanocomposites reinforced with cellulose nanofibers. *Polymer Bulletin*, *75*(5), 2039–2051. https://doi.org/10.1007/s00289-017-2142-8

Xu, S., Girouard, N., Schueneman, G., Shofner, M. L., & Meredith, J. C. (2013). Mechanical and thermal properties of waterborne epoxy composites containing cellulose nanocrystals. *Polymer*, *54*(24), 6589–6598. https://doi.org/10.1016/j.polymer.2013.10.011

Yuan, T., Zeng, J., Wang, B., Cheng, Z., & Chen, K. (2021). Lignin containing cellulose nanofibers (LCNFs): Lignin content-morphology-rheology relationships. *Carbohydrate Polymers*, *254*. https://doi.org/10.1016/j.carbpol.2020.117441

Yue, L., Ke, K., Amirkhosravi, M., Gray, T. G., & Manas-Zloczower, I. (2021). Catalyst-Free Mechanochemical Recycling of Biobased Epoxy with Cellulose Nanocrystals. *ACS Applied Bio Materials*, *4*(5), 4176–4183. https://doi.org/10.1021/acsabm.0c01670

Yusra, A. F. I., Khalil, H. P. S. A., Sohrab Hossain, M., Davoudpour, Y., Astimar, A. A., Zaidon, A., Dungani, R., & Mohd Omar, A. K. (2015). Epoxy nanocomposites. In *BioResources* (Vol. 10, Issue 4).

Yusuf, J., Sapuan, S. M., Rashid, U., Ilyas, R. A., & Hassan, M. R. (2024). Thermal, mechanical, and morphological properties of oil palm cellulose nanofibril reinforced green epoxy nanocomposites. *International Journal of Biological Macromolecules*, *278*. https://doi.org/10.1016/j.ijbiomac.2024.134421

Zhang, X., Kitin, P., Agarwal, U. P., Gleisner, R., & Zhu, J. Y. (2023). Characterizing lignin-containing microfibrillated cellulose based on water interactions, fibril properties, and imaging. *Carbohydrate Polymers*, *316*. https://doi.org/10.1016/j.carbpol.2023.120996

Zhang, Y., Nypelö, T., Salas, C., Arboleda, J., Hoeger, I. C., & Rojas, O. J. (2013). Cellulose nanofibrils: From strong materials to bioactive surfaces. *Journal of Renewable Materials*, *1*(3), 195–211. https://doi.org/10.7569/JRM.2013.634115

Chapter 3

Optimization of Extrusion Parameters for Wood Flour-Epoxy Composites with Potential Additive-Manufacturing Applications in Construction

3.1 Abstract

The sustainable utilization of wood waste is critical for reducing environmental impact and advancing eco-friendly construction materials. This study investigates the optimization of extrusion parameters—specifically wood flour particle size, extrusion rates, and wood content—in the fabrication of epoxy resin and wood flour composites designed for extrusion-based 3D printing. Through a factorial experimental design, the effects of these parameters on mechanical, physical, and fire-resistant properties were systematically evaluated. Characterization included flexural and compressive strength tests, water absorption, dimensional stability, and fire resistance assessments. Statistical analyses revealed that the epoxy-to-wood ratio is the most influential factor, with a 55:45 ratio yielding optimal results: enhanced mechanical strength, improved dimensional stability, and superior fire resistance, while minimizing surface defects. These findings underscore the pivotal role of precisely optimizing extrusion parameters to produce high-performance, sustainable composites suitable for additive manufacturing in construction. The results contribute valuable insights toward developing wood-based materials capable of replacing petroleum-derived materials, supporting both environmental responsibility and enhanced material performance in the building industry.

Keywords*: Wood–epoxy composites; Extrusion parameters; Additive-Manufacturing; Construction materials.*

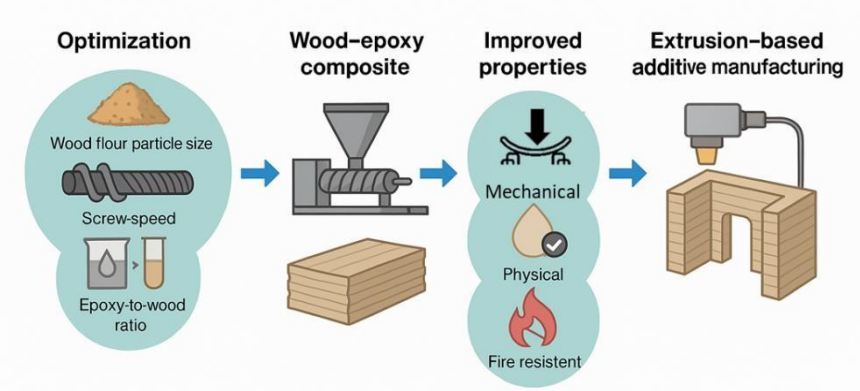

Fig. 3.1 Schematic Overview of the Experimental Design for Wood–Epoxy Composites

3.2 Introduction

Wood is an abundant resource that has been widely adopted in various aspects of daily life due to its exceptional mechanical properties (Arias et al., 2022). Increased population and human activity promoted the utilization of wood resources, which has generated a massive amount of waste wood or wood residue. In 2018, the United States Environmental Protection Agency (EPA) reported that a total of 18.1 million tons of wood were accumulated in municipal solid waste (MSW), which accounted for 6.2 percent of all MSW generated that year. Additionally, nearly 12.2 million tons of this wood waste was disposed of in landfills without any further use (U.S. Environmental Protection Agency [EPA], 2024) Thus, it is necessary to make effective use of waste wood products to reduce the negative effects on the environment, as well as improve the economics of the lumber industry overall, through adding value to underutilized wood sources. To further encourage ecologically beneficial activities and reduce greenhouse gas emissions, there is now a global push to promote eco-friendly building materials (Rosa Latapie et al., 2023). Large quantities of inconsistent wood processing waste are typically produced during industrial wood treatment, and these waste materials can be utilized as resources to develop wood products with superior qualities, independent of their size variations (Nguyen et al., 2023; Yan et al., 2024).

3D printing, often known as additive manufacturing (AM), is a cutting-edge industrial production technique that utilizes computer-aided design software for layer-by-layer printing of target materials with

complex 3D structure (ISO/ASTM, 2015; Trovato et al., 2025; Lamm et al., 2020). Recently, extrusion-based additive manufacturing (AM) has gained popularity as a method for fabricating dimensional parts and design concepts, even for extremely complex designs. Compared to liquid and powder-based AM methods, extrusion-based AM includes additional design flexibility, higher manufacturing magnitude, and more affordable production. Originally developed for polymer filaments, this technology now combines less-extrudable materials with polymers that enhance extrusion. (Altıparmak et al., 2022). Several types of wood products originating from hardwood and softwoods are being investigated for use in 3D printing composite formulations. Lamm et al. have summarized the use of wood flours, sawdust, and barks, and lignocellulosic fillers used in extrusion AM processing. To obtain composites, typical polymer categories such as poly-lactic acid, polypropylene, urea-formaldehyde, polyvinyl acetate, styrene maleic anhydride copolymer, and poly-lactic acid are widely mixed with wood particles (Lamm et al., 2020).

Thermosetting polymers are preferred over thermoplastics for construction purposes due to their greater creep, resistance to heat, and energy efficiency (Carne et al., 2023). However, the application of wood and thermosets was not widely investigated in the context of 3D printing technology. Using an extrusion method, Orji et al. combined wood with sodium silicate to create two-dimensional rods. The 1:1 blend showed strong flexural, thermal, and fire performance, while curing temperature significantly affected the flexural strength and water resistance of wood–sodium silicate rods (Orji et al., 2023). In a separate investigation, the same research team investigated the possibility of using softwood mill wastes (50–90%) in additive manufacturing (AM) of wood composite materials using two thermosetting resins: urea-formaldehyde (UF) and phenol-resorcinol-formaldehyde (PRF) resin. The rheological characteristics of the wood-PRF (50:50) blend permitted effective extrusion, whereas the inadequate viscosity and moisture content of the wood-UF mixtures prevented extrusion. Developing an extrudable wood composite for additive manufacturing required selecting a suitable resin and wood-resin mix that cures at room temperature (Orji & McDonald, 2023).

Epoxy resin is one of the most commercially relevant polymeric materials and has been the subject of extensive research, numerous patents, and a wide range of scientific and technical innovations over the

years (Sienkiewicz & Czub, 2023). The extrusion method is more effective than injection molding when processing composite materials with wood flour content. However, the extrusion of wood, plastic, or resin presents several challenges, including non-uniform feeding, frequent flow instabilities, surface tearing, and serious melt fractures (Mazzanti & Mollica, 2020). Some researchers have used wood material and epoxy in extrusion-based research. Yousef Jahani utilized a twin-screw extruder to create composites of wood flour and polypropylene by combining epoxy resin with 30 and 40 weight percent wood flour and polypropylene. With a surge in epoxy resin content, it was found that composites' tensile strength dropped while their elastic modulus and absorption of water improved (Jahani, 2007). Feng et al. have investigated how epoxy resin affects the mechanical, rheological, and water absorption rates of composites made of wood flour and high-density polyethylene (HDPE). They found that the quantity of epoxy resin in the composites improves their tensile, flexural, and impact qualities up to a certain limit before declining (Feng et al., 2018). A few studies used epoxy as a surface treatment agent for wood-plastic extruded composite.

For example, Mohamed et al. applied epoxy as an adhesive coating on wood plastic composites (WPC) produced by extruding wood flour and virgin polyethylene with a coupling agent. (Mohamed et al., 2019). Gramlich et al. applied epoxy surface treatment to extruded WPCs made from pine wood flour and polypropylene after various pre-treatments. (Gramlich et al., 2006). Although the combination of wood and epoxy resin has been the subject of numerous studies, there is a notable lack of research that focuses only on wood and epoxy resin, which offers an opportunity for thorough investigation.

This study will focus on optimizing extrusion parameters for epoxy resin and wood flour composites. The particle size of wood flour, extrusion rates, and wood content will all be changed to determine their effects on the process. A factorial experimental design will be used to determine the best combination of these parameters and evaluate the mechanical and physical performance of the resultant composites. One of the primary concerns with wood-based construction materials is their low fire safety and reduced thermal stability (Seo et al., 2016). According to Pan et al., combining epoxy resin with wood aerogel treated with a flame-retardant coating made from polyethyleneimine, melamine, and phytic acid can enhance the flame resistance and thermal stability of wood-epoxy composites. When the treated wood

aerogel was incorporated into the epoxy resin, the researchers observed the formation of an ordered network within the epoxy matrix of the wood-epoxy composite. This three-dimensional network may be responsible for the improved flame resistance of the wood-epoxy composite compared to pure epoxy resin (Pan et al., 2024). Consequently, this study also incorporates fire testing of wood-epoxy extruded composites. The findings from this research have the potential to significantly benefit the scientific community by advancing the development of sustainable wood-based composites that reduce the use of petroleum-based plastics. The thorough property analysis can pave the way for wood-based construction systems that prioritize both environmental responsibility and performance.

3.3 Materials and methods

3.3.1 Materials

Southern yellow pine (SYP) sawmill residues in the form of wood flakes were sourced from Huber Engineered Woods (Georgia, USA). The flakes were oven-dried at 103 ± 2 °C until reaching constant weight, then ground using a Thomas-Wiley Laboratory Mill, Model 4 (Thomas Scientific, USA) fitted with 0.5 mm and 1 mm screens. The ground material was sieved through a 40-mesh U.S. standard screen, and the fraction passing through (under 40 mesh) was collected, homogenized, and stored in sealed containers for later use. The epoxy system consisted of a diglycidyl ether of bisphenol A (DGEBA) resin, Epon 828, supplied by Hexion Inc. (USA). This resin contains two epoxide groups and has an epoxide equivalent weight of 185–192 g/eq. At 25 °C, its viscosity is 110–150 P and its density is 1.16 g/cm³. The curing agent used was polyoxypropylene diamine (D-400), acquired from Everchem Specialty Chemicals (USA), with a molecular weight of approximately 430 g/mol and an amine hydrogen equivalent of 4.41 meq/g. At 20 °C, D-400 exhibits a viscosity of 0.22 P and a density of 0.972 g/cm³.

3.3.2 Composite Extrudates Preparation

Epon 828 and Jeffamine D-400 were first mixed at a weight ratio of 100:55. Wood flour (under 40 mesh, with a moisture content of 2–3%) was then added to the resin mixture. Composite formulations were prepared with resin-to-wood weight ratios of 40:60, 45:55, 50:50, 55:45, and 60:40. The mixtures were blended using a food processor (Hamilton Beach model 70730, 450 W, 10-cup capacity) for 5 minutes to ensure homogeneous dispersion. The mixtures were processed using an SJ35 single-screw extruder (RobotDigg, Shanghai, China) with a 35 mm barrel diameter and 420 mm barrel length. A 13.5 mm diameter mild steel die was securely attached to the extruder's barrel outlet. The extrusion process utilized a 5 mm pitch screw, designed by the Department of Mechanical Engineering at Idaho University for this project (**Figure 3.2**). The wood-epoxy mixture blend was manually fed into the extruder and processed for 3 minutes at three different screw speeds, 40, 60, and 80 rpm, to produce extruded rods. Finally, the rods were allowed to cure for 24 hours at 35 °C in the oven. After this time, the post-curing process was carried out at 105 °C for 2 hours and finally at 120 °C for 1 hour. Five specimens were constructed for each set of epoxy:wood and screw speed combinations. A total of 75 rods were fabricated for different testing.

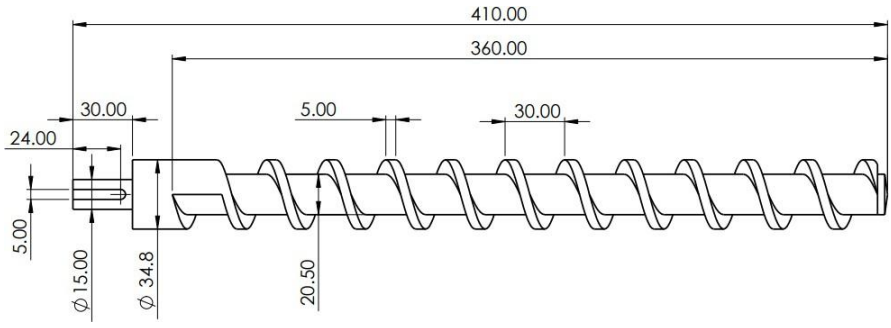

Fig. 3.2 Dimensions of the custom-designed screw used in the extrusion experiments. Design provided by the Department of Mechanical Engineering at the University of Idaho. Special thanks to Conal Thie and Robert Carne for their support with the screw design.

3.3.3 Composite Extrudates Characterization

3.3.3.1 Particle Size Distribution (Sieve Analysis)

A sieve analysis was conducted on 200 g samples of wood flour that had been previously ground and screened through either 0.5 mm or 1 mm mesh screens. The material, which passed through a 40-mesh sieve, was analyzed using a standard mechanical shaker for 10 minutes. Each sample was passed through a stack of U.S. standard sieves with mesh sizes 40, 60, 80, 100, and 200 to assess the particle size distribution.

3.3.3.2 Mechanical Testing

Extruded wood–epoxy composite rods were evaluated for flexural strength (three-point bending) and compressive strength in accordance with ASTM D1037. The mechanical tests were performed using a Zwick/Roell universal testing machine (Instron Zwick/Roell, Germany) equipped with a 10 kN load cell, operating at a crosshead speed of 5 mm/min.

3.3.3.3 Water Absorption and Dimensional Stability

Water absorption and dimensional stability of the extruded wood–epoxy rods (10 mm in length) were evaluated after 24 hours of immersion in water at 23 ± 1 °C, following the procedures outlined in ASTM D570. After soaking, excess surface water was removed with a dry cloth, and the specimens were immediately weighed to determine the wet mass. Water absorption was calculated as the percentage increase in weight. Dimensional changes were measured using a digital caliper to assess radial swelling.

3.3.3.4. Fire Resistance Test

A fire test was performed on cured rods in triplicate. Samples were exposed to the tip of the Bunsen burner flame (1000–1100 °C) and monitored for 5 minutes via an IR camera, with the mass loss of the samples continuously recorded by a load cell. Images taken from the video were analyzed at one-minute intervals to evaluate physical changes in the samples, and final weight loss was recorded. The fire test setup, designed by the Departments of Aerospace Engineering and Forestry at Auburn University, includes a load

cell for mass loss measurement, an IR camera, and a propane flow rate controller. The test was conducted with a propane mass flow rate of 7.5 SLM, positioning the samples 30.48 cm from the flame base at 1000 °C, and extended for a total duration of 7 minutes.

3.3.3.5 Statistical Analysis

For the statistical analysis in this study, a combination of factorial and single-factor experimental approaches was employed to evaluate the effects of processing parameters and material formulation on the performance of wood–epoxy composites. In experiments involving two independent variables—such as screw speed and particle size, or epoxy-to-wood ratio and screw speed—a full factorial design was implemented. The resulting data were analyzed using two-way ANOVA to examine both main effects and interaction effects. For other characterizations, including water absorption and swelling, one-way analyses were conducted to assess the impact of a single variable. Following the ANOVA, Duncan's test was applied to identify statistically significant differences between group means. All statistical analyses were performed by the author using R software (version 4.4.3) and evaluated at a 95% confidence level (5% significance level). This integrated experimental strategy enabled a comprehensive evaluation of how processing and formulation parameters influence the composites' mechanical, physical, and fire-resistance properties.

3.4 Results and discussion

3.4.1 Particle Size Distribution of Wood Flour

The screened wood flour, with a moisture content of 5.2%, was analyzed for particle size distribution. The results of the sieve analysis are shown in **Figure 3.3.** For both the 0.5 mm and 1 mm screens (particles retained under 40 mesh), the 40–60 mesh fraction had the highest weight percentage, especially for the 1 mm screen. In the case of the 0.5 mm screen, the weight percentage of 60–100 mesh

particles was 27 w/w% higher compared to the 1 mm screen. Additionally, the 60–80 mesh fraction represented 40 w/w% of the particles for the 0.5 mm screen, while it was only 17% for the 1 mm screen.

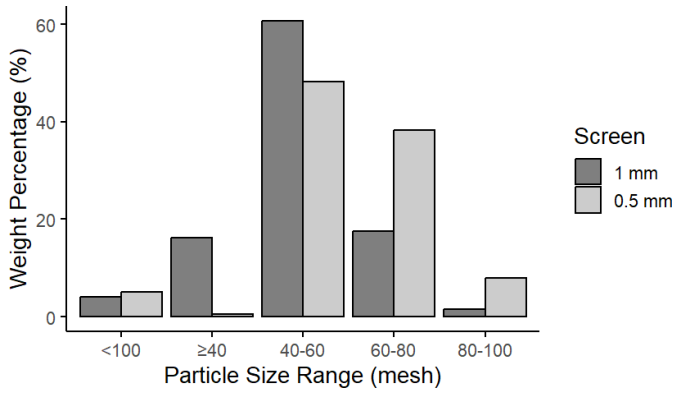

Fig. 3.3 Wood particle size distribution from the under 40 mesh screened wood flour

3.4.2. Formulation Selection for Mechanical Characterization

To ensure a representative baseline for evaluating mechanical performance, the 50:50 epoxy-to-wood flour ratio was selected as the reference formulation for initial testing. This intermediate ratio was chosen because it lies at the midpoint of the broader range explored in subsequent analyses (40:60, 45:55, 50:50, 55:45, and 60:40). By starting with a balanced formulation, we aimed to establish a central data point from which the influence of increasing or decreasing epoxy content could be more clearly interpreted. This selection also allowed for consistent comparisons when assessing the effects of other parameters, such as wood particle size and screw speed.

3.4.3 Mechanical Characterization of Extruded Composite Samples

3.4.3.1 Elastic Modulus and Compressive Strength of Extruded Composites as a Function of Particle Size

Elastic modulus and compressive strength of the 50:50 Epoxy to wood composite rods as a function of wood particle size (1 mm and 0.5 mm screens) and screw speed (40, 60, and 80 rpm) are shown in **Figure 3.4** Statistical data analysis revealed that, for both properties, the main effects of particle size and screw

speed were not statistically significant, as indicated by p-values well above the 0.05 threshold. However, while the interaction effect was not significant for elastic modulus ($p = 0.151$), it was statistically significant for compressive strength ($p = 0.0137$), suggesting that the combined influence of particle size and screw speed plays a critical role in determining this property. Specifically, at 40 rpm, larger particles (1 mm) resulted in higher compressive strength and elastic modulus, whereas at higher screw speeds (60 and 80 rpm), finer particles (0.5 mm) enhanced the mechanical performance—highlighting the importance of processing conditions in optimizing composite properties. This interaction effect aligns with previous research showing that finer particles, under suitable extrusion conditions, tend to improve composite strength due to better flow, dispersion, and matrix integration.

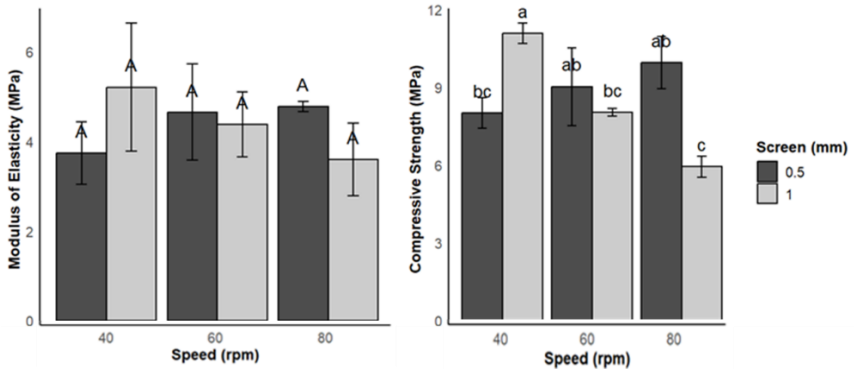

Fig. 3.4 Modulus of Elasticity (Left) and Compressive Strength (Right) as a function of Screen Size and Speed.

Note: Uppercase letters indicate significant differences in Modulus of Elasticity means, and lowercase letters indicate significant differences in Compressive Strength means. Different letters (a, b, c, etc.) indicate statistically significant differences between means according to Duncan's multiple range test ($p < 0.05$). Means sharing at least one letter (e.g., ab' or 'bc') are not significantly different.

Miki et al. (2003) reported that the fluidity of wood powder decreases with increasing particle size, which can hinder the extrusion process. In contrast, finer particles enhance the compaction and consolidation of wood composites, as demonstrated by Chaudemanche et al. (2018), likely contributing to improved mechanical strength in this study. From a processing standpoint, both the mechanical properties

and fiber morphology of wood composites are strongly influenced by extrusion parameters such as screw configuration and material composition (Matuana & Li, 2004). Similarly, Migneault et al. (2008) observed that composites containing shorter fibers generally exhibit superior mechanical performance, primarily due to their more uniform dispersion within the polymer matrix. These findings are consistent with the current results, where finer particles combined with higher screw speeds resulted in enhanced compressive strength, suggesting that improved compaction and dispersion under higher shear conditions positively influence mechanical behavior.

In conventional wood–polymer composites, particle size remains a critical factor in determining mechanical behavior. Several studies have reported that increasing wood particle size can enhance properties such as flexural, tensile, and compressive strength, as well as hardness (Jasiński et al., 2025; Madhoushi et al., 2014; Stark & Berger, n.d.). Wood flour is typically characterized by mesh size, which defines the range of particle sizes obtained through screening.

While smaller particles can improve the uniformity of the composite and increase the available surface area for interfacial bonding (Golmakani et al., 2021)—thereby facilitating better stress transfer throughout the material—a similar trend was observed by Ratanawilai et al. (2014), who reported that the compressive strength and modulus of composites slightly increased as particle size decreased. This enhancement was attributed to the more homogeneous distribution of smaller particles within the polymer matrix, which improved the material's capacity to bear compressive loads. In the present study, the optimized particle size was 0.5 mm, which outperformed the larger 1 mm particles in terms of compressive strength, particularly at higher screw speeds (60 and 80 rpm). This suggests that finer particles enable better dispersion and compaction under increased shear conditions during extrusion, leading to a more cohesive internal structure and enhanced mechanical performance. Therefore, optimizing particle size—especially toward smaller sizes like 0.5 mm—is essential to achieving an effective balance between processing efficiency and mechanical reinforcement in extruded wood-epoxy composites.

3.4.3.2 Elastic Modulus and Flexural Strength as a Function of Ratios

Flexural strength and modulus of elasticity of wood –epoxy composites as a function of epoxy-to-wood ratio (40:60, 45:55, 50:50, 55:45, and 60:40) and screw speed (40, 60, and 80 rpm) are shown in **Figure 3.5** The results indicate that flexural strength increases with higher epoxy content, with the 55:45 and 60:40 formulations exhibiting the highest values. At lower epoxy levels (40:60 and 45:55), flexural strength remained relatively low across all screw speeds. Notably, the 55:45 and 60:40 composites showed marked improvements at 60 rpm, reaching ~26 MPa and ~29 MPa, respectively. This suggests that a moderate screw speed (60 rpm) may optimize matrix dispersion and interfacial bonding due to a balance between shear and residence time (Zhang et al., 2012). Interestingly, although 40 rpm should provide longer residence time, the same improvement was not observed at this lower speed. This discrepancy could be due to insufficient shear energy at 40 rpm, which may limit effective dispersion and wetting of wood particles. However, the exact reason remains unclear and may involve additional factors such as material backflow, pressure fluctuations, among others (Duretek et al., 2015; Gebhard et al., 2023).

Similarly, the modulus of elasticity increased with both the epoxy content and screw speed, reaching a maximum of 19.6 GPa at the 60:40 ratio and 80 rpm. These results indicate that increasing the epoxy proportion significantly enhances composite stiffness and strength. This finding aligns with previous studies reporting that higher wood content in polymer matrices typically reduces mechanical properties, such as flexural strength and modulus of elasticity, due to weaker interfacial bonding at higher filler loadings (Nukala et al., 2022; Yang et al., 2012). Although higher screw speeds promote better matrix flow and shear-induced dispersion, excessively high speeds can reduce the residence time (Zhang et al., 2009), potentially limiting effective wetting and stress transfer at the interface, ultimately leading to a decrease in mechanical performance. Additionally, at higher screw speeds for the 60:40 blend, the formation of *sharkskin*—a surface defect characterized by periodic roughness or ridges on the extrudate—was observed. This phenomenon is caused by a stick-slip mechanism at the die exit, which occurs when the material experiences critical levels of shear stress and acceleration, leading to surface instabilities (Thie, 2021). The

presence of sharkskin negatively impacts the surface finish and may further contribute to the reduction in mechanical properties.

Statistical analysis supported these observations. The main effect of the epoxy-to-wood ratio was highly significant for both flexural strength and modulus of elasticity ($p < 0.001$), indicating that material composition strongly influences mechanical behavior. Screw speed also showed a significant effect on modulus of elasticity ($p = 0.00426$) and a marginal effect on flexural strength ($p = 0.0964$). However, the interaction between ratio and screw speed was not statistically significant for either property ($p = 0.503$ for MOE; $p = 0.537$ for flexural strength), suggesting that the effects of these two factors are largely independent within the tested range**.**

On the other hand, the effect of screw speed on composite density was not statistically significant ($p = 0.973$) (**Table 3.1**), nor was the interaction between screw speed and the epoxy-to-wood ratio ($p = 1.000$). These results indicate that variations in screw speed did not meaningfully influence the material's density under the tested conditions. This finding is consistent with previous research, which reported that screw speed has a limited impact on the final density of polymer-based composites (Chevali & Ulven, 2012).

In contrast, the epoxy-to-wood ratio exhibited a highly significant main effect on density ($p < 0.001$), highlighting the dominant role of formulation in determining the compactness of the composite (Chen et al., 2006). This supports the notion that increasing the proportion of epoxy results in a denser material, likely due to enhanced matrix continuity and reduced void formation (Siddikur Rahman et al., 2018). Overall, these findings underscore that material composition, rather than processing speed, is the key factor in controlling composite density.

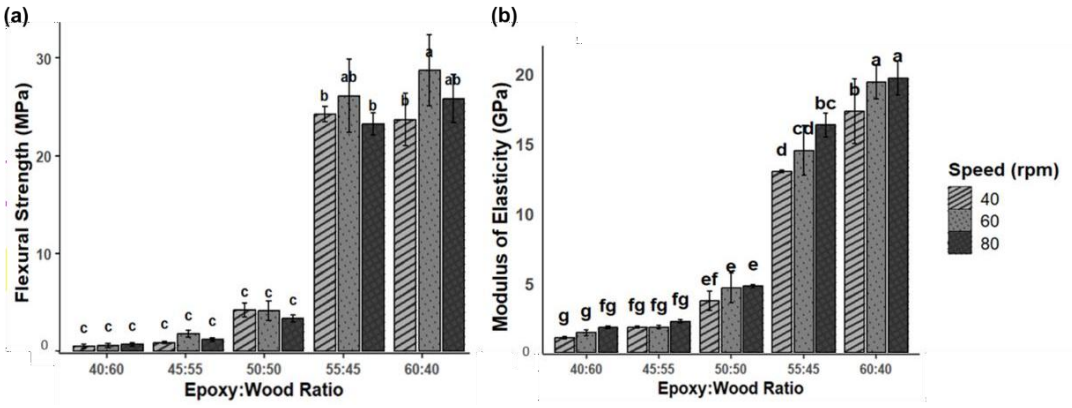

Fig. 3.5 *Flexural Strength* (a) and *Modulus of Elasticity* (b) of the extruded composites.

Note: Different lowercase letters within each panel denote statistically significant differences among treatments according to Duncan's multiple range test (α = 0.05). Letter assignments are independent for each panel and should not be compared across graphs.

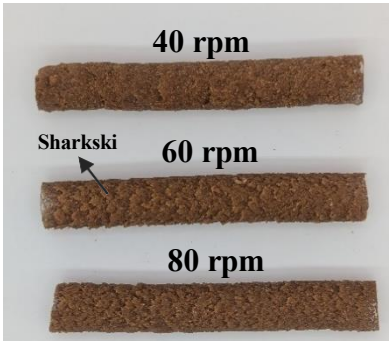

Fig. 3.6 Epoxy-to-wood (60:40) rods after extrusion at different speeds

Table 3.1 Effect of screw speed and epoxy-to-wood ratio on composite density (g/cm³)

Ratio	**Density (g/cm³)**		
	Screw Speed (rpm)		
Epoxy:Wood	**40**	**60**	**80**
40:60	0.60±0.01	0.68±0.02	0.72±0.01
45:55	0.65±0.005	0.67±0.01	0.77±0.01
50:50$_S$	0.69±0.03	0.73±0.003	0.71±0.02

50:50$_b$	0.64±0.01	0.72±0.01	0.76 ±0.002
55:45	0.76±0.01	0.97±0.02	0.98±0.02
60:40	1.05±0.005	0.99±0.01	0.97±0.01

Note: S: Small screen (0.5 mm); b: big screen (1 mm)

Figure 3.7 shows a clear positive trend in compressive strength parallel to the rod's length as the epoxy content in the epoxy: wood ratio increases. As the epoxy content increases, the material shows greater compressive strength. This improvement could be due to epoxy's high inherent strength (Guo et al., 2022).and its ability to enhance bonding and distribute loads more evenly within the composite, leading to better mechanical performance under axial compression.

The results of the two-way ANOVA confirmed this effect, showing that the epoxy:wood ratio had a highly significant impact on compressive strength ($p < 0.001$). Additionally, screw speed also had a significant effect ($p < 0.01$), although to a lesser extent. The interaction between ratio and screw speed was not statistically significant ($p = 0.18$), indicating that their effects on compressive strength were mostly independent.

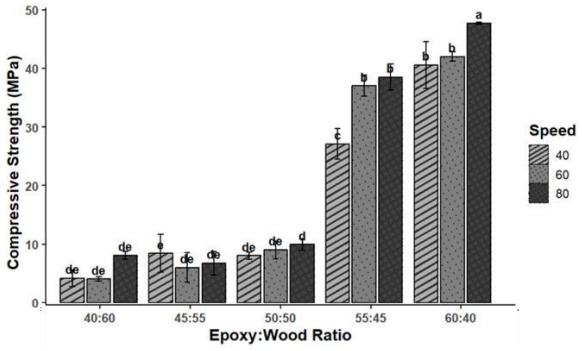

Fig. 3.7 Compressive properties of the extruded composites.

Note: Different lowercase letters indicate statistically significant differences among treatments based on Duncan's multiple range test at α = 0.05.

3.4.4 Water Absorption and Dimensional Stability

Water absorption and radial swelling were evaluated in relation to screw speed and the epoxy-to-wood flour ratio (see **Table 3.2**). An initial analysis of variance (ANOVA) revealed that screw speed had no statistically significant effect on either property ($p > 0.05$). In contrast, the epoxy-to-wood flour ratio significantly influenced both water absorption and swelling, highlighting the importance of formulation in controlling moisture-related behavior. To better isolate and characterize the influence of the ratio, water absorption values were averaged across different screw speeds for each ratio. This approach allowed a clearer assessment of the effect of the epoxy-to-wood flour ratio on water absorption, independent of the extrusion speed.

The results showed a general decrease in water absorption and radial swelling with increasing resin content. Specifically, water absorption remained remarkably low for the 55:45 and 60:40 resin-to-wood flour ratios. Although both ratios exhibited reduced radial swelling, the 55:45 ratio performed comparably—or even slightly better—than the 60:40 ratio. These findings are consistent with trends reported in the literature. It is well established that increasing resin content in wood–plastic composites (WPCs) significantly reduce water absorption and swelling. Yang et al. (2012) reported that WPCs with 60% wood content displayed the highest water uptake, which continued beyond 24 hours of immersion. In contrast, our composites with higher resin content (55:45 and 60:40) maintained water absorption below 4% after 24 hours, demonstrating the effectiveness of increased resin proportions in limiting moisture uptake.

This behavior can be attributed to better encapsulation of wood particles and enhanced interfacial adhesion between the hydrophilic wood flour and the hydrophobic epoxy matrix (Khan et al., 2019). The improved matrix coverage reduces the exposure of wood pores to water, thereby lowering water absorption. Furthermore, as noted by Migneault et al. (2008), larger wood particles and higher wood content tend to increase water absorption due to incomplete polymer coverage. These observations support our conclusion that a higher resin proportion (i.e., a lower wood content) is key to improving the water and swelling resistance of these composites.

Table 3.2 Average values of water absorption and radial swelling for composites after 24 hours of soaking.

Ratio	Physical properties	
Epoxy:Wood	**Absorption (%)**	**Swelling (%)**
40:60	45.01±5.28	6.65±1.30
45:55	36.59±4.88	4.99±1.01
50:50s	27.67±4.42	4.89±0.75
50:50$_b$	27.93±0.78	4.97±0.59
55:45	5.04±0.72	1.45±0.22
60:40	2.10±0.53	1.63±0.11

Note: S: Small screen (0.5 mm); b: big screen (1 mm)

3.4.5 Fire Resistance Evaluation of the Composite Rods

Mass loss and flame spread rate of wood–epoxy composites as a function of epoxy-to-wood ratio and screw speed are shown in **Figure 3.8** Mass loss reflects the amount of material consumed during combustion, indicating overall flammability, while flame spread rate represents the speed at which fire propagates across the composite surface, providing insight into fire resistance (Xu et al., 2019). The results showed that mass loss decreased with increasing resin-to-wood ratios, indicating that composites with a higher resin content are less flammable due to improved char formation and thermal protection. Statistical analysis using one-way ANOVA confirmed that the effect of the wood ratio on mass loss was highly significant ($p < 0.001$), demonstrating that varying the wood content substantially influences the composite's flammability. Similarly, the flame spread rate was also significantly affected by the epoxy-to-wood ratio ($p < 0.001$), confirming that resin content plays a critical role in enhancing fire resistance.

Based on the flame spread rate graphs and maximum temperature distribution, it was observed that the maximum temperature spread over a smaller surface area in rods with a 55:45 epoxy-to-wood ratio

compared to other compositions. Although the flame spread rate generally decreased with increasing resin content, the rods with a 60% epoxy composition showed higher flame spread rates. This suggests that beyond a certain resin concentration, fire behavior may be influenced by other factors, such as the thermal degradation pattern of the resin itself. Additionally, the presence of "sharkskin" at higher screw speeds and epoxy contents (see **Figure 3.6**) may also contribute to the increased flame spread rate in these samples. Sharkskin leads to a rougher, less smooth surface, which can create micro-defects (Arda & Mackley, 2005) and localized heat concentration, facilitating ignition and flame propagation. Particle size did not show a significant impact on flame performance.

Natural fiber-reinforced polymer composites face a significant limitation due to their thermal instability. Both the polymer matrix and natural fibers are inherently flammable, acting as effective conductors of fire. The high flammability of natural fibers is largely attributed to their high cellulose content, which ignites more readily than components with higher hemicellulose or lignin content (Saba et al., 2016). In this context, increasing the wood flour ratio leads to greater mass loss during thermal degradation. Interestingly, composites with the highest epoxy-to-wood ratio (60:40) also exhibited considerable mass loss. This may be related to the decomposition behavior of epoxy, which, as a thermosetting polymer, breaks down at elevated temperatures (typically between 400–500 °C), releasing heat, smoke, soot, and toxic volatiles (Rakotomalala et al., 2010). Therefore, optimizing the resin-to-fiber ratio is essential not only to improve mechanical performance but also to enhance flame resistance and ensure the development of safer and more sustainable composite materials.

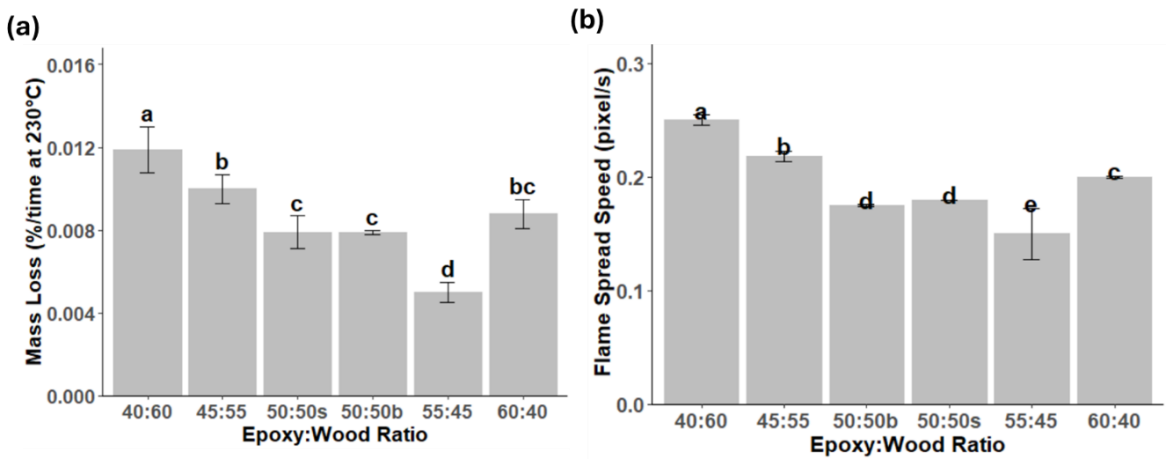

Fig. 3.8 Influence of epoxy-to-wood ratio on (a) mass loss and (b) flame spread rate of the composites during the fire test.

Note: S: Small screen (0.5 mm); b: big screen (1 mm). Different lowercase letters within each panel denote statistically significant differences among treatments according to Duncan's test (α = 0.05). Letter assignments are independent for each panel and should not be compared across graphs.

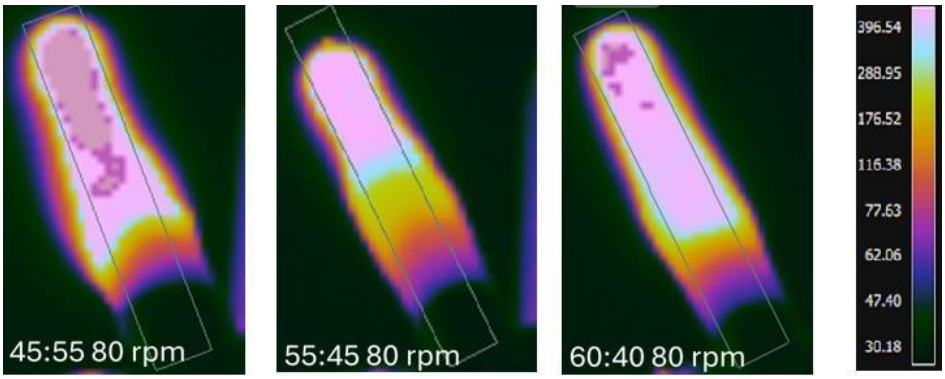

Fig. 3.9 Infrared thermal monitoring of cured rods subjected to a Bunsen burner flame

3.5 Conclusions

This study demonstrated that the epoxy-to-wood ratio is the most critical factor influencing the physical, mechanical, and fire-resistant properties of extruded wood–epoxy composites. Among the tested ratios, the 55:45 epoxy-to-wood ratio provided the best overall performance, significantly enhancing compressive strength, flexural strength, and stiffness due to optimal bonding and effective encapsulation of wood particles. Higher epoxy content at this ratio also contributed to reduced water absorption and radial swelling, leading to improved dimensional stability thanks to more complete resin coverage. Additionally, fire resistance was enhanced, as evidenced by lower mass loss and slower flame spread. Furthermore, maintaining a balanced epoxy-to-wood ratio like 55:45 is crucial to avoid surface defects such as sharkskin. In conclusion, the 55:45 epoxy-to-wood ratio is key for producing extruded wood–epoxy composites with superior mechanical, physical, and fire-resistant properties while ensuring surface quality and dimensional stability.

3.6 References

Altıparmak, S. C., Yardley, V. A., Shi, Z., & Lin, J. (2022). Extrusion-based additive manufacturing technologies: State of the art and future perspectives. *Journal of Manufacturing Processes*, *83*, 607–636. https://doi.org/10.1016/J.JMAPRO.2022.09.032

Arda, D. R., & Mackley, M. R. (2005). The effect of die exit curvature, die surface roughness and a fluoropolymer additive on sharkskin extrusion instabilities in polyethylene processing. *Journal of Non-Newtonian Fluid Mechanics*, *126*(1), 47–61. https://doi.org/10.1016/j.jnnfm.2004.12.005

Arias, A., Feijoo, G., & Moreira, M. T. (2022). New Environmental Approach Based on a Combination of Planetary Boundaries and Life Cycle Assessment in the Wood-Based Bioadhesive Market. *ACS Sustainable Chemistry & Engineering*, *10*(34), 11257–11272. https://doi.org/10.1021/acssuschemeng.2c03058

Carne, R. H. R., Alade, A. A., Orji, B. O., Ibrahim, A., McDonald, A. G., & Maughan, M. R. (2023). A screw extrusion-based system for additive manufacturing of wood: Sodium silicate thermoset composites. *Advances in Mechanical Engineering*, *15*(11). https://doi.org/10.1177/16878132231210373/ASSET/279F82D7-FF5C-4F3A-9280-227A2D1D8EBC/ASSETS/IMAGES/LARGE/10.1177_16878132231210373-FIG9.JPG

Chaudemanche, S., Perrot, A., Pimbert, S., Lecompte, T., & Faure, F. (2018). Properties of an industrial extruded HDPE-WPC: The effect of the size distribution of wood flour particles. *Construction and Building Materials*, *162*, 543–552. https://doi.org/10.1016/j.conbuildmat.2017.12.061

Chen, H. C., Chen, T. Y., & Hsu, C. H. (2006). Effects of wood particle size and mixing ratios of HDPE on the properties of the composites. *Holz Als Roh - Und Werkstoff*, *64*(3), 172–177. https://doi.org/10.1007/s00107-005-0072-x

Chevali, V. S., & Ulven, C. A. (2012). Effect of extrusion screw speed on biocomposite thermo-mechanical properties. *International Journal of Sustainable Engineering*, *5*(1), 38–46. https://doi.org/10.1080/19397038.2010.547625

Duretek, I., Schuschnigg, S., Gooneie, A., Langecker, G. R., & Holzer, C. (2015). Rheological properties of wood polymer composites and their role in extrusion. *Journal of Physics: Conference Series*, *602*(1). https://doi.org/10.1088/1742-6596/602/1/012014

Feng, C., Li, Z., & Wang, H. (2018). The effect of epoxy resin on wood-plastic composites. *Pigment and Resin Technology*, *47*(5), 369–376. https://doi.org/10.1108/PRT-05-2017-0052/FULL/PDF

Gebhard, J., Schulze, A., Clausmeyer, T., & Tekkaya, A. E. (2023). Continuous hot extrusion with a stationary valve. *CIRP Annals*, *72*(1), 237–240. https://doi.org/10.1016/j.cirp.2023.03.003

Golmakani, M. E., Wiczenbach, T., Malikan, M., Aliakbari, R., & Eremeyev, V. A. (2021). Investigation of wood flour size, aspect ratios, and injection molding temperature on mechanical properties of wood flour/polyethylene composites. *Materials*, *14*(12). https://doi.org/10.3390/ma14123406

Gramlich, W. M., Gardner, D. J., & Neivandt, D. J. (2006). Surface treatments of wood–plastic composites (WPCs) to improve adhesion. *Journal of Adhesion Science and Technology*, *20*(16), 1873–1887. https://doi.org/10.1163/156856106779116623

Guo, D., Guo, N., Fu, F., Yang, S., Li, G., & Chu, F. (2022). Preparation and mechanical failure analysis of wood-epoxy polymer composites with excellent mechanical performances. *Composites Part B: Engineering*, *235*. https://doi.org/10.1016/j.compositesb.2022.109748

ISO/ASTM. (2015, diciembre 15). ISO/ASTM 52900:2015 (E) – Additive manufacturing — General principles — Terminology [International Standard]. ISO. Retrieved June 23, 2025, from https://www.iso.org/obp/ui/#iso:std:iso-astm:52900:ed-2:v1:en

Jahani, Y. (2007). The effect of epoxy-polyester hybrid resin on mechanical properties, rheological behavior, and water absorption of polypropylene wood flour composites. *Polymer Engineering and Science*, *47*(12), 2041–2048. https://doi.org/10.1002/PEN.20917;JOURNAL:JOURNAL:15482634;WGROUP:STRING:PUBLICATION

Jasiński, W., Szymanowski, K., Nasiłowska, B., Barlak, M., Betlej, I., Prokopiuk, A., & Borysiuk, P. (2025). 3D Printing Wood–PLA Composites: The Impact of Wood Particle Size. *Polymers*, *17*(9). https://doi.org/10.3390/polym17091165

Khan, M. Z. R., Srivastava, S. K., & Gupta, M. K. (2019). Water absorption and its effect on mechanical properties of hybrid wood particulates composites. *Materials Research Express*, *6*(10). https://doi.org/10.1088/2053-1591/ab34c3

Lamm, M. E., Wang, L., Kishore, V., Tekinalp, H., Kunc, V., Wang, J., Gardner, D. J., & Ozcan, S. (2020). Material Extrusion Additive Manufacturing of Wood and Lignocellulosic Filled Composites. *Polymers 2020, Vol. 12, Page 2115*, *12*(9), 2115. https://doi.org/10.3390/POLYM12092115

Madhoushi, M., Rafighi, A., Dorostkar, A., & Madhoushi, M. (2014). Investigation on mechanical properties of composite made of sawdust and high density Polyethylene. In *International Journal of Lignocellulosic Products* (Vol. 1, Issue 2). http://ijlp.gau.ac.ir

Matuana, L. M., & Li, Q. (2004). Statistical Modeling and Response Surface Optimization of Extruded HDPE/Wood-Flour Composite Foams. *Journal of Thermoplastic Composite Materials*, *17*(2), 185–199. https://doi.org/10.1177/0892705704035404

Mazzanti, V., & Mollica, F. (2020). A review of wood polymer composites rheology and its implications for processing. In *Polymers* (Vol. 12, Issue 10, pp. 1–23). MDPI AG. https://doi.org/10.3390/polym12102304

Thie, C. S. (2021). *Wood and resin composite extrusion for additive manufacturing* [Master's thesis, University of Idaho]. University of Idaho Library. https://objects.lib.uidaho.edu/etd/pdf/Thie_idaho_0089N_12197.pdf

Migneault, S., Koubaa, A., Erchiqui, F., Chaala, A., Englund, K., Krause, C., & Wolcott, M. (2008). Effect of fiber length on processing and properties of extruded wood-fiber/HDPE composites. *Journal of Applied Polymer Science*, *110*(2), 1085–1092. https://doi.org/10.1002/app.28720

Miki, T., Takakura, N., Iizuka, T., Yamaguchi, K., & Kanayama, K. (2003). Possibility of extrusion of wood powders. *JSME International Journal Series A Solid Mechanics and Material Engineering*, *46*(3), 371-377. DOI:10.1299/jsmea.46.371

Mohamed, M. R., Naguib, H. M., El-Ghazawy, R. A., Shaker, N. O., Amer, A. A., Soliman, A. M., & Kandil, U. F. (2019). Surface Activation of Wood Plastic Composites (WPC) for Enhanced Adhesion with Epoxy Coating. *Materials Performance and Characterization*, *8*(1), 22–40. https://doi.org/10.1520/MPC20180034

Nguyen, D. L., Luedtke, J., Nopens, M., & Krause, A. (2023). Production of wood-based panel from recycled wood resource: a literature review. *European Journal of Wood and Wood Products*, *81*(3), 557–570. https://doi.org/10.1007/S00107-023-01937-4/TABLES/4

Nukala, S. G., Kong, I., Kakarla, A. B., Tshai, K. Y., & Kong, W. (2022). Preparation and Characterisation of Wood Polymer Composites Using Sustainable Raw Materials. *Polymers*, *14*(15). https://doi.org/10.3390/polym14153183

Orji, B. O., & McDonald, A. G. (2023). Flow, curing and mechanical properties of thermoset resins–wood-fiber blends for potential additive-manufacturing applications. *Wood Material Science and Engineering*, *18*(4), 1487–1504. https://doi.org/10.1080/17480272.2022.2155873;SUBPAGE:STRING:ACCESS

Orji, B. O., Thie, C., Baker, K., Maughan, M. R., & McDonald, A. G. (2023). Wood fiber - sodium silicate mixtures for additive manufacturing of composite materials. *European Journal of Wood and Wood Products*, *81*(1), 45–58. https://doi.org/10.1007/S00107-022-01861-Z/METRICS

Pan, Y., Wang, W., Zhang, D., Lü, T., & Zhao, H. (2024). Construction of a continuous flame-retardant network made from wood in epoxy resin. *Cellulose*, *31*(13), 8311–8319. https://doi.org/10.1007/S10570-024-06069-3/FIGURES/5

Rakotomalala, M., Wagner, S., & Döring, M. (2010). Recent developments in halogen free flame retardants for epoxy resins for electrical and electronic applications. *Materials*, *3*(8), 4300–4327. https://doi.org/10.3390/ma3084300

Ratanawilai, T., Nakawirot, K., Deachsrijan, A., & Homkhiew, C. (2014). Influence of wood species and particle size on mechanical and thermal properties of wood polypropylene composites. *Fibers and Polymers*, *15*(10), 2160–2168. https://doi.org/10.1007/s12221-014-2160-1

Rosa Latapie, S., Lagouin, M., Sabathier, V., & Abou-Chakra, A. (2023). From aggregate to particleboard: A new multi-scale model approach to thermal conductivity in bio-based materials. *Journal of Building Engineering*, *78*, 107664. https://doi.org/10.1016/J.JOBE.2023.107664

Saba, N., Jawaid, M., Paridah, M. T., & Al-othman, O. Y. (2016). A review on flammability of epoxy polymer, cellulosic and non-cellulosic fiber reinforced epoxy composites. In *Polymers for Advanced Technologies* (Vol. 27, Issue 5, pp. 577–590). John Wiley and Sons Ltd. https://doi.org/10.1002/pat.3739

Seo, H. J., Kim, S., Huh, W., Park, K. W., Lee, D. R., Son, D. W., & Kim, Y. S. (2016). Enhancing the flame-retardant performance of wood-based materials using carbon-based materials. *Journal of Thermal Analysis and Calorimetry*, *123*(3), 1935–1942. https://doi.org/10.1007/S10973-015-4553-9/FIGURES/8

Sienkiewicz, A., & Czub, P. (2023). Functional Management of Waste Wood Flour as an Example of a 'Greener' Approach towards the Synthesis of Bio-Based Epoxy Resins. *Polymers 2023, Vol. 15, Page 3521*, *15*(17), 3521. https://doi.org/10.3390/POLYM15173521

Stark, N. M., & Berger, M. J. (1997). *Effect of Particle Size on Properties of Wood-Flour Reinforced Polypropylene Composites*. https://www.fpl.fs.usda.gov/documnts/pdf1997/stark97d.pdf

Trovato, M., Belluomo, L., Bici, M., Prist, M., Campana, F., & Cicconi, P. (2025). Machine learning in design for additive manufacturing: A state-of-the-art discussion for a support tool in product design lifecycle. *The International Journal of Advanced Manufacturing Technology 2025 137:5*, *137*(5), 2157–2180. https://doi.org/10.1007/S00170-025-15273-9

U.S. Environmental Protection Agency. (2024, November 8). Wood: Material-specific data. In Facts and figures about materials, waste and recycling. U.S. Environmental Protection Agency. Retrieved June 23, 2025, from https://www.epa.gov/facts-and-figures-about-materials-waste-and-recycling/wood-material-specific-data

Xu, Y., Lv, C., Shen, R., Wang, Z., & Wang, Q. (2019). Experimental investigation of thermal properties and fire behavior of carbon/epoxy laminate and its foam core sandwich composite. *Journal of Thermal Analysis and Calorimetry*, *136*(3), 1237–1247. https://doi.org/10.1007/s10973-018-7735-4

Yan, J., Yang, C., Xue, B., Zhang, T., & Qu, W. (2024). 3D microstructural characterization and mechanical properties determination of poplar-ultrathin fiberboard. *Construction and Building Materials*, *432*, 136662. https://doi.org/10.1016/J.CONBUILDMAT.2024.136662

Yang, T. H., Leu, S. Y., Yang, T. H., & Lo, S. F. (2012). Optimized material composition to improve the physical and mechanical properties of extruded wood-plastic composites (WPCs). *Construction and Building Materials*, *29*, 120–127. https://doi.org/10.1016/j.conbuildmat.2011.09.013

Zhang, J., Park, C. B., Rizvi, G. M., Huang, H., & Guo, Q. (2009). Investigation on the uniformity of high-density polyethylene/wood fiber composites in a twin-screw extruder. *Journal of Applied Polymer Science*, *113*(4), 2081–2089. https://doi.org/10.1002/app.29991

Zhang, Z. X., Gao, C., Xin, Z. X., & Kim, J. K. (2012). Effects of extruder parameters and silica on physico-mechanical and foaming properties of PP/wood-fiber composites. *Composites Part B: Engineering*, *43*(4), 2047–2057. https://doi.org/10.1016/j.compositesb.2012.01.047

Chapter 4

Effect of Partial Replacement of Phenol-Resorcinol-Formaldehyde Resin with Bio-oil on Thermal, Mechanical, and Curing Properties

4.1 Abstract

In the present study, the effect of partially replacing a commercial phenol-resorcinol-formaldehyde (PRF) resin with bio-oil, at substitution levels up to 50%, was investigated with respect to its thermal, mechanical, and curing (pot life) properties. The curing behavior was analyzed by differential scanning calorimetry (DSC), and thermal stability was assessed via thermogravimetric analysis (TGA). Pot life was estimated through gelation time measurements. Mechanical performance was evaluated using three-point bending tests to determine flexural strength and modulus. Results showed that the addition of bio-oil slowed the curing kinetics, particularly at lower temperatures; however, this effect could be partially mitigated by increasing the curing temperature. Thermal stability decreased with a higher bio-oil content due to the presence of less stable bio-oil components, but remained adequate for practical use. Flexural testing revealed that neat PRF cured at 120 °C had the highest strength and stiffness. Partial substitution with 30% bio-oil caused moderate reductions in mechanical properties, while 50% substitution significantly reduced strength and stiffness and induced a ductile, flexible failure mode. This study highlights the potential of bio-oil to partially replace phenol in PRF resins, offering a pathway toward more sustainable adhesives with tunable performance based on formulation and curing conditions.

Keywords: *Bio-based resins; flexural performance; curing behavior*

4.2 Introduction

Phenol-formaldehyde (PF) resins have been used for decades as adhesives in the manufacture of wood-based products such as plywood, fiberboard, and particleboard (Ayrilmis & Özbay, 2017). These resins are synthesized through the polymerization of phenol and formaldehyde in the presence of a catalyst (Berdnikova et al., 2021). Due to their low reactivity, PF resins typically require the use of a hardener and are generally cured under hot-pressing conditions at temperatures above 160 °C (Ayrilmis & Özbay, 2017; T. Li et al., 2017).

For this reason, the development of adhesives capable of curing at room temperature, commonly referred to as cold-setting adhesives, has gained significant attention. These adhesives are not only safer to handle but also considerably reduce energy consumption and operational costs in wood product manufacturing (Wibowo et al., 2025; Wibowo & Park, 2024). One alternative to conventional PF resins is phenol-resorcinol-formaldehyde (PRF) resins, which can be cured at room temperature under neutral conditions due to their high reactivity (Liu et al., 2017). These resins form strong bonds and perform exceptionally well under various weathering conditions (Lisperguer et al., 2005). Cold-setting PRF adhesives are typically produced in two steps. First, a low-condensation PF resol with reactive methylol groups is synthesized by reacting phenol with excess formaldehyde under alkaline conditions. Then, resorcinol is added, reacting with the PF methylol groups to form a thermosetting PRF resin with resorcinol grafted onto the PF chain. Curing is driven by a cross-linking polycondensation reaction between excess resorcinol and the added formaldehyde hardener (Kläusler et al., 2013). However, PRF resins are generally more expensive than conventional PF resins (Liu et al., 2017), and their rapid curing at room temperature can limit the processing window in applications that involve mixing, pressing, or extrusion with wood materials (Wibowo & Park, 2024).

A promising strategy to extend this pot life and reduce production costs is the partial replacement of phenol with lignocellulosic biomass or its liquefied bio-oil in the preparation of phenolic resins (Dong et al., 2018; Faraheen Kabir Ahmad et al., 2022). Biomass is a key renewable source of energy and chemical feedstocks, offering a sustainable alternative to fossil-based resources (Kircher, 2015). Among biomass

conversion technologies, fast pyrolysis stands out for its thermochemical efficiency, producing a bio-oil rich in phenolic compounds, making it an ideal candidate for chemical production (Cui et al., 2017). Several studies have explored the feasibility of partially replacing phenol with biomass-derived bio-oil in PF resin formulations, highlighting its lower cost and renewable origin (Sarika et al., 2020). For instance, research involving bio-oil obtained from sugarcane bagasse pyrolysis demonstrated that substitution levels up to 20% did not compromise shear strength, which remained comparable to that of commercial resins (Faraheen et al., 2022). Similarly, Ayrilmis & Özbay (2017) reported enhancements in mechanical properties such as wet shear strength, modulus of rupture (MOR), and modulus of elasticity (MOE) in plywood bonded with resins modified with 20% bio-oil.

In addition, Q. Li et al. (2020) showed that PF resins modified with phenol-rich bio-oil significantly improved the mechanical performance of panels, achieving up to a 13% increase in bond strength compared to unmodified resins, even at substitution levels of up to 50%. In another study by Cui et al. (2017b), a bio-oil-modified PF (BPF) resin containing 20% bio-oil exhibited only a slight effect on its curing behavior. In their study, thermal analyses, including DSC and TGA, indicated that while the addition of bio-oil altered the curing process, performance remained largely unaffected at low substitution levels. Furthermore, improvements in bending strength suggested a positive influence of bio-oil on the mechanical properties of the resin. In a separate study, Ren et al. (2017) synthesized a bio-oil-resorcinol-aldehyde (BRF) resin by partially replacing resorcinol with pyrolysis bio-oil. As the proportion of bio-oil increased, both the viscosity and solid content of the resin also increased. However, this modification resulted in a decrease in shear strength. Despite this, at substitution levels of up to 20%, the mechanical strength and wood failure values remained comparable to those of conventional resorcinol-formaldehyde (RF) resins. Although extensive research has been conducted on the partial replacement of phenol with bio-oil in phenolic resins, few studies have explored this substitution in commercially available PRF resins, particularly focusing on their curing behavior and mechanical properties in structural applications.

In the present study, the effect of partially replacing a commercial phenol-resorcinol-formaldehyde (PRF) resin with bio-oil, at substitution levels of up to 50%, was investigated with respect to its thermal,

mechanical, and curing (pot life) properties. The curing behavior was analyzed using differential scanning calorimetry (DSC), and thermal stability was assessed by thermogravimetric analysis (TGA). Pot life was estimated through gelation time measurements. To evaluate the structural performance of the modified adhesives, three-point bending tests were conducted to determine the flexural modulus and flexural strength. These techniques provided insights into the influence of bio-oil content on the overall performance of the modified adhesive.

4.3 Materials and Method

4.3.1 Materials

The bio-oil used in this study, derived from the pyrolysis of pine sawdust waste, was produced at the Center for Bioenergy and Bioproducts, Auburn University, Alabama. According to Sakhakarmy et al. (2024), the bio-oil used in this study had a pH of 3.5 and a water content of 13.56%, with hydroxyl group concentrations of 4.20 mmol/g for aliphatic OH, 3.96 mmol/g for phenolic OH, and 0.53 mmol/g for acidic OH, resulting in a total OH concentration of 8.69 mmol/g. The commercial resins used were cold-setting phenol-resorcinol-formaldehyde (PRF) systems, Cascophen™ 4001-8 (resin) and Cascoset 5830 E (hardener), supplied by Hexion. These were combined in a 2.5:1 ratio of resin to hardener, yielding a system with a pH of 10.2. The specific gravities of the components were 1.181 for Cascophen 4001-8 and 1.209 for Cascoset 5830 E.

4.3.2 Preparation of PRF- Bio-oil matrix

For the preparation of the resin with partial bio-oil replacement, the dry material of each component was first measured, as shown in **Table 4.1.** Based on these values, the amount of bio-oil required to partially replace Cascophen was calculated. The three components, bio-oil, Cascophen, and Cascoset, were combined simultaneously. The mixture was stirred using a magnetic stirrer at 500 RPM for 5 min.

Table 4.1 Dry material content of the resin components

Sample	Average Dry Material Content (wt.%)
Bio oil	50.40
Cascophen	57.92
Cascoset	16.92

4.3.3 Characterization of Resin Curing Behavior of liquid sample

4.3.3.1 Differential Scanning Calorimetry (DSC)

Differential Scanning Calorimetry (DSC) analysis was performed on the liquid resin samples to study their curing behavior and thermal transitions. The DSC tests provided insight into the exothermic curing reactions at different bio-oil substitution levels and curing temperatures. Samples of 5 to 10 mg were placed in aluminum pans and scanned under a controlled heating program from 25 °C to 170 °C at a rate of 10 °C/min in a nitrogen flow of 50 mL/min. Based on the DSC results—particularly the onset and peak temperatures of the exothermic curing reactions—the appropriate curing temperature parameters were selected for each formulation. This thermal characterization was essential to define curing profiles while

carefully staying within a temperature range that avoids potential resin degradation. These parameters were subsequently used to guide the selection of curing temperatures in the full factorial experimental design, allowing for a systematic evaluation of the effect of temperature and bio-oil content on resin performance.

4.3.3.2 Gel Time Measurement

A 6 g sample of resin was placed into a 15 mm diameter glass vial, into which a glass rod was also inserted. The vial was then immersed in an oil bath maintained at a controlled temperature range of 60–120 ± 1 °C. The gel time was recorded as the elapsed time from the moment the vial was immersed in the oil bath until the resin reached gelation, identified by the formation of a continuous resin thread adhering to the glass rod when it was gently lifted from the resin.

4.3.4 Characterization of Resin Curing Behavior of cured samples

4.3.4.1 Thermogravimetric Analysis (TGA)

The thermogravimetric analyses (TGA) of cured resin samples were performed using a TA Instruments Q500 analyzer to evaluate their thermal stability. Prior to testing, all samples were cured and dried at 105 °C overnight to remove residual moisture. Approximately 10 to 20 mg of each specimen was placed in platinum crucibles and heated from 30 °C to 900 °C at a rate of 10 °C/min under a nitrogen atmosphere with a flow rate of 50 mL/min. The thermogravimetric (TG) and derivative thermogravimetric (DTG) curves were recorded to analyze the thermal decomposition behavior.

4.3.5 Full Factorial Experimental Design

In our experiment, we used a full factorial design to quantitatively assess the relationship between the response functions and the process variables, specifically examining the influence of curing temperatures and % Bio-oil on the curing process of bio-based phenol-resorcinol-formaldehyde (PRF) resin. The variables identified were:

(a) Curing temperature, x_1

(b) % Bio-oil, x_2,

The Curing temperature was varied systematically to evaluate its impact on the resin's performance. Three different Curing temperatures were tested: 60, 90, and 120 °C. Two-response parameters, namely, Flexural Strength and Modulus, were used to characterize the curing response of the system. **Table 4.2** shows the experimental ranges and levels of the factors used in the full factorial design.

The number of runs (N) required for a full factorial design is determined using the formula provided by Wang & Wan (2009).

$$\mathbf{N} = L_1 \times L_2 \times \ldots \times L_3$$

where :

$L_1 \times L_2 \times \ldots \times L_3$ is the number of levels for each factor,

In our experiment:

L_1 (Curing temperature) = 3

L_2 (% Bio-oil) = 3

Therefore, the total number of runs (N) required is:

$$\boldsymbol{N}=3\times3=9$$

Table 4.2 Experimental ranges and levels of the factors used in the full factorial design.

Factor	Units	Levels Tested
Curing Temperature	°C	60, 90, 120
Bio-oil Substitution	%	0, 30, 50

4.3.6 Mechanical Testing Procedure

Mechanical testing was conducted to evaluate the flexural properties of cured resin samples in accordance with ASTM D790 — *Standard Test Methods for Flexural Properties of Unreinforced and Reinforced Plastics and Electrical Insulating Materials*. Rectangular specimens with uniform dimensions of 127 mm (length) × 12.7 mm (width) × 3.2 mm (thickness), as specified by the standard, were fabricated using silicone molds supplied by MB Prototyping Ltd. (Canada). All samples were tested using a three-point bending setup under consistent conditions.

4.3.6.1 Optimization of Curing Time for Neat PRF Resin

To identify the optimal curing duration for the neat phenol-resorcinol-formaldehyde (PRF) resin, gel time measurements were initially performed. Based on these results, three curing durations—3×, 5×, and 10× the measured gel time—were selected for evaluation. For each condition, four replicate specimens were prepared and tested using the three-point bending method to determine flexural strength and modulus. A one-way analysis of variance (ANOVA) was conducted to examine the influence of curing duration on mechanical performance. Where statistically significant differences were detected ($p < 0.05$), Duncan's multiple range test was applied to identify homogeneous groups. The condition corresponding to 10× the gel time resulted in significantly superior mechanical properties and was therefore selected for all subsequent tests.

4.3.6.2 Mechanical Testing of Bio-Oil-Modified Formulations

The optimized curing condition (10× gel time) was applied to all bio-oil-modified PRF formulations. These included various bio-oil loadings and were cured at three target temperatures—60°C, 90°C, and 120°C—as defined by the experimental matrix. For each condition, four replicate specimens were prepared and tested under identical three-point bending conditions. A two-way ANOVA was conducted to evaluate the effects of curing temperature and bio-oil content on flexural properties. When significant differences were observed, Duncan's multiple range test was used to identify statistically distinct groups.

4.3.6.3 Differential Scanning Calorimetry (DSC) Analysis of Cured Samples

DSC was performed on cured neat PRF and bio-oil modified resins (30% and 50%) using the same equipment and parameters as for liquid samples. Approximately 5–10 mg of each sample were heated from 25 °C to 170 °C at 10 °C/min under nitrogen flow (50 mL/min). The thermograms were analyzed to assess residual curing and crosslinking efficiency after curing at 60 °C, 90 °C, and 120 °C.

4.4 Results and Discussion

4.4.1 Curing Behavior and Thermal Stability of PRF–Bio-oil Resin Systems

4.4.1.1 Differential Scanning Calorimetry (DSC)

Figure 4.1 shows the DSC thermograms of the pure PRF resin, pure bio-oil, and mixtures with 30% and 50% substitution of PRF by bio-oil. In all cases, a first exothermic shoulder appears around 60–130 °C. This peak has been attributed to the reaction of the 4 and 6 positions of the resorcinol ring with formaldehyde, leading to the formation of mono-, di-, and tri-hydroxymethyl derivatives, precursors of the subsequent crosslinking. In some studies, this reaction shows a maximum around 85 °C (Chow, 1997; Kinnertová & Slovák, 2018). This is followed by a second endothermic peak, which has been attributed to water loss during the formation of the crosslinked network (Liu et al., 2020; Wang et al., 1994). These results agree with previous studies that distinguish between a first exothermic event associated with the formation of reactive precursors and a second endothermic event related to water loss during the formation of the crosslinked network.

In the pure PRF sample, the main endothermic peak occurs at 135.87 °C; for the formulation with 30% bio-oil, this peak shifts slightly to 139.08 °C, suggesting that bio-oil addition increases the energy required for the polymerization process. In the 50% bio-oil sample, the endothermic peak becomes broader and less defined, which may indicate reduced crosslinking efficiency due to the presence of less reactive components in the bio-oil (Shahid et al., 2015).

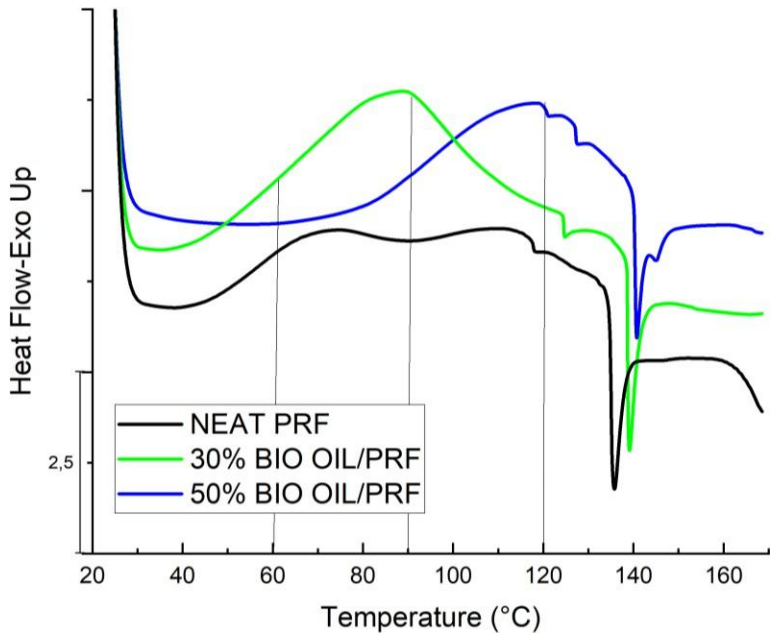

Fig. 4.1 Thermograms by DSC of PRF resins with varying bio-oil substitution levels to assess curing behavior and thermal transition.

Based on these thermal analysis results, three curing temperatures 60 °C, 90 °C, and 120 °C were selected to conduct a full factorial design using the three formulations (pure PRF, 30% bio-oil substitution, and 50% bio-oil substitution). These temperatures were chosen to capture the range of critical thermal events. This comprehensive approach helps in understanding not only how the presence of bio-oil affects the crosslinking efficiency but also provides practical insights into the processing and performance of the adhesive formulations under varied thermal curing conditions.

4.4.1.2 Curing Behavior Assessed by Gelation Time Measurements

Table 4.3 presents the gelation times of neat PRF and bio-oil-modified resin formulations at curing temperatures of 60, 90, and 120 °C, illustrating the effects of both temperature and bio-oil content on the curing kinetics. Gel time, defined as the point at which a three-dimensional polymer network begins to form, reflects the onset of crosslinking (Celikbag et al., 2020).

As expected, gelation times decreased with increasing temperature for all formulations, indicating accelerated crosslinking under higher thermal input. Neat PRF consistently exhibited the shortest gel times across all temperatures, confirming its high reactivity. In contrast, the incorporation of bio-oil significantly extended gelation times, particularly at lower temperatures, suggesting that certain components in the bio-oil may hinder or delay network formation. The most pronounced delay was observed in the 50% bio-oil formulation at 60 °C. However, this inhibitory effect diminished at elevated temperatures: at 120 °C, the gelation times of the 30% and 50% bio-oil formulations were reduced to 1.53 and 5.04 minutes, respectively.

These results suggest that while bio-oil reduces the system's reactivity—likely due to the presence of less reactive or interfering compounds—this effect can be partially mitigated by increasing the curing temperature, which enhances the overall curing process. This trend is consistent with previous studies on bio-based phenolic systems, where partial replacement with bio-oil initially accelerates curing, but higher substitution levels significantly prolong gelation time due to the lower reactivity and reduced number of reactive sites in bio-oil compared to phenol (Celikbag et al., 2020; Dong et al., 2018; KOKTEN et al., 2020).

Table 4.3 Gelation time of neat PRF and bio-oil-modified resin formulations at three curing temperatures.

Formulation	Temperature (°C)	Gelation Time (min)
Neat PRF		3.93±0.02
30% Bio-Oil / PRF	60	8.89±0.27
50% Bio-Oil / PRF		133.35±14
Neat PRF		1.60±0.02
30% Bio-Oil / PRF	90	2.93±0.02
50% Bio-Oil / PRF		14.77±0.07
Neat PRF		1.10±0.02
30% Bio-Oil / PRF	120	1.53±0.03
50% Bio-Oil / PRF		5.04±0.26

Based on the gelation time results, curing time estimations were established by evaluating fixed multiples of the measured gelation times (specifically 3×, 5×, and 10×) for each temperature and formulation. These curing schedules were tested to determine the minimum duration required to achieve a stable and fully crosslinked polymer network. The effectiveness of each condition was assessed using differential scanning calorimetry (DSC) and mechanical testing. Among the evaluated conditions, a curing time equivalent to 10× the gelation time consistently produced fully cured materials across all resin systems, offering a reliable balance between processing time and network completion. Therefore, this multiplier was adopted as the basis for defining the curing schedule in the subsequent composite fabrication and property evaluations. This approach is consistent with previous studies in thermoset processing, where gelation—identified by the crossover of G′ and G″ is used as a reference point to estimate complete cure (Tung & Dynes, 1982).

4.4.2 Thermal Stability of Bio-oil /PRF–Resin Systems (TGA)

The thermal stability of the PRF adhesives modified with bio-oil was evaluated using TGA, and the results are presented in **Figure 4.2**. The thermograms exhibit three main degradation events, with a clear trend of decreasing thermal stability as bio-oil content increases. This is evidenced by the reduction in both the onset degradation temperature—defined as the temperature at 5% weight loss—and the maximum degradation temperature (Tmax). For the unmodified adhesive (neat PRF), the onset degradation temperature was 183.1 °C and the Tmax was 314.3 °C. In contrast, the formulation with 30% bio-oil showed an onset at 144.9 °C and Tmax at 217.2 °C, while the 50% bio-oil formulation presented a slightly higher onset at 158.4 °C but a lower Tmax of 187.9 °C. These findings indicate that increasing bio-oil content compromises the thermal resistance of the resin, likely due to the presence of thermally labile components in the bio-oil.

For the neat PRF, the first thermal degradation event occurred between 200 and 360 °C. This stage is primarily attributed to the evaporation of free water and moisture, along with the release of low molecular weight compounds formed during the condensation reaction, such as free formaldehyde and phenol. It may

also involve the cleavage of terminal groups from the polymer chains (Liu et al., 2017b; Wang et al., 2009). The corresponding weight loss in this region results from the physical desorption of water and the emission of volatile compounds, including cresols and other small aromatics (Cui et al., 2017).

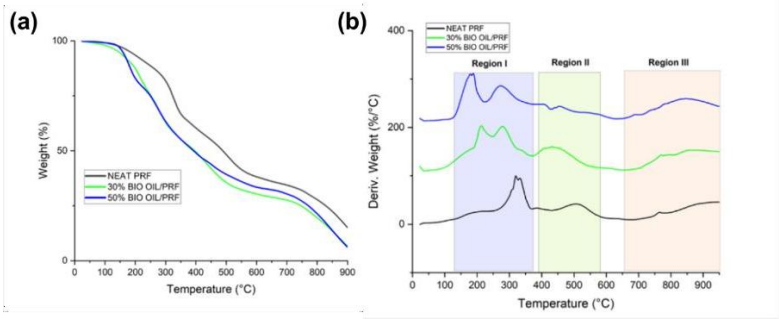

Fig 4.2 TGA (a) and DTG (b) Curves of PRF Adhesives with Varying Bio-Oil Content.

In the samples containing 30% and 50% bio-oil, the first degradation event shifts to a lower temperature range (approximately 120–356 °C), indicating that thermal degradation begins earlier compared to the neat resin. This observation is supported by the decrease in onset degradation temperatures, which drop from 183.1 °C for the neat PRF to 144.9 °C and 158.4 °C for the 30% and 50% bio-oil formulations, respectively. This behavior is likely attributed to the incorporation of thermally less stable compounds present in the bio-oil. Nevertheless, the thermal stability of the bio-oil-modified PRF resins remains acceptable, as evidenced by the residual carbon content at 900 °C: 36.09% for the 30% bio-oil formulation and 28.5% for the 50% formulation, compared to 38.4% for the neat PRF. These values suggest that, despite a reduction in initial thermal stability with increasing bio-oil content, a considerable amount of char remains after thermal decomposition. For phenolic resins, the formation of residual carbon (char) is particularly important, as it reflects the presence of highly crosslinked aromatic structures that are resistant to thermal degradation (Sun & Sun, 2020).

The second thermal region, located between ~400 and 600 °C for all formulations, is associated with the decomposition of methylene and ether bridges within the polymer network. These reactions release phenol, cresol homologs, and other aromatic compounds (Cui et al., 2017; Wang et al., 2009). Additionally,

the cleavage of these bonds generates methylene and hydroxyl radicals, which may undergo further oxidation to form carbonyl and carboxyl groups. The degradation in this region also contributes to the release of gases such as CH_4, CO, and CO_2. A small quantity of benzene and its derivatives may also form due to the breakdown of methylene and ether bridges. Moreover, reactions involving phenolic hydroxyl groups and methylene or two hydroxyl groups can lead to water release Cui et al., 2017). The third thermal region, observed above 650 °C, is related to the further degradation of aromatic structures, mainly due to the dehydrogenation of benzene rings leading to carbonaceous residue formation (Lee et al., 2012).

These thermal degradation results, when considered alongside the DSC and gelation time data, confirm that increasing bio-oil content alters the curing behavior and reduces the thermal stability of PRF resins. The shifts in exothermic and endothermic transitions observed in DSC, as well as the prolonged gelation times, suggest that the incorporation of bio-oil delays and weakens the crosslinking process. Consequently, the resulting polymer networks exhibit lower thermal resistance, as evidenced by earlier degradation onset and reduced Tmax in TGA. Despite these changes, the presence of substantial char yields indicates that a thermally stable, aromatic-rich structure is still formed, especially at moderate bio-oil substitution levels.

4.4.3 Flexural Properties of Bio-oil /PRF–Resin Systems

4.4.3.1 Curing Time Optimization Using Neat PRF Resin

As shown in **Figure 4.3**, the effect of curing time (3×, 5×, and 10× gelation time) on the mechanical properties of neat PRF resin was evaluated in terms of flexural strength (MOR) and flexural modulus (MOE). This analysis aimed to determine the curing duration that maximizes crosslinking efficiency and mechanical performance without overextending the curing process. The observed trend indicates a clear improvement in both MOR and MOE with increasing curing time, particularly at 60 °C.

Statistical analysis confirmed that curing time had a significant effect on flexural strength (MOR), with a p-value of 0.0244, indicating that at least one group's MOR was significantly different from the others ($p < 0.05$). Increasing the gelation time multiplier from 3× to 10× led to a statistically significant

improvement in flexural strength, with the highest value observed at 10× gelation time. Notably, there was no significant difference between 3× and 5×, both of which resulted in lower MOR values compared to 10×.

In terms of stiffness (flexural modulus, MOE), 10× gelation time also resulted in the best mechanical performance. Although the MOE at 5× was slightly lower than at 10×, the difference was not statistically significant. However, curing at only 3× gelation times significantly reduced mechanical performance, especially in terms of MOE. These results suggest that a minimum of 5× the gelation time is required to achieve acceptable strength and stiffness, while 10× provides the optimal curing condition for neat PRF resin under the tested parameters.

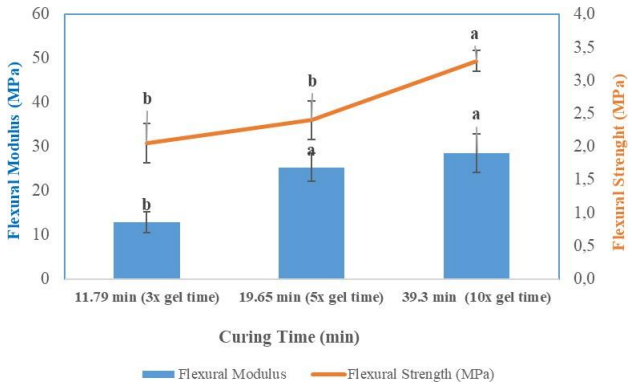

Fig. 4.3 Flexural strength (MOR) and flexural modulus (MOE) of neat PRF resin cured at 3×, 5×, and 10× gelation time at 60 °C.

Note: Bars represent mean values with error bars indicating standard deviation (n = 4). Different letters indicate statistically significant differences between groups ($p < 0.05$).

Based on the mechanical performance results of neat PRF resin at different curing times, the curing duration equivalent to 10× the gelation time was selected for subsequent experiments. This condition provided the highest flexural strength and modulus, indicating optimal crosslinking and structural integrity. Therefore, to ensure consistent curing and allow meaningful comparison across formulations, the 10× gelation time was adopted as the standard curing duration for evaluating the effect

of curing temperature. For each temperature condition (60 °C, 90 °C, or 120 °C), the corresponding curing time was calculated based on the gelation time previously determined at that temperature.

4.4.4 Evaluation of Modified Formulations Using the Selected Curing Time

4.4.4.1 Assessment of Cure Completion by DSC

Differential Scanning Calorimetry (DSC) thermograms of cured neat PRF and bio-oil-modified resins (30% and 50% substitution) cured at 60 °C, 90 °C, and 120 °C are presented in **Figure 4.4.** These profiles provide insights into the extent of curing and the residual thermal activity in the networks after thermal treatment.

For the neat PRF formulation, the DSC curve of the sample cured at 60 °C exhibits a noticeable exothermic shoulder around 80–130 °C. This thermal event is associated with residual curing reactions, indicating that the crosslinking process was not fully completed under this curing condition. As the curing temperature increases to 90 °C and 120 °C, the intensity of this exothermic event progressively decreases, which is consistent with previous findings regarding the increased degree of cure at higher temperatures (Solomon & Rudin, 1990). The sample cured at 120 °C exhibits the lowest residual heat flow, suggesting that a more complete polymerization was achieved under this condition. The formulation containing 30% bio-oil substitution exhibits a similar thermal behavior to neat PRF. The sample cured at 60 °C shows a noticeable exothermic shoulder, indicative of partial curing. However, unlike neat PRF, the exothermic shoulder persists in the sample cured at 120 °C, although with reduced intensity. This suggests that the incorporation of bio-oil decreases the curing efficiency, likely due to the presence of less reactive components, which increase the energy required for complete network formation (Shahid et al., 2015).

In the case of 50% bio-oil substitution, the thermograms display broader and less defined exothermic transitions across all curing temperatures. These features imply a lower degree of curing and a less homogeneous polymer network. Residual exothermic activity is still evident at 120 °C, supporting the idea that the high bio-oil content significantly interferes with the crosslinking process. The broadness and persistence of these thermal events may also be attributed to the increased presence of non-phenolic or

aliphatic compounds within the bio-oil, which show lower reactivity toward formaldehyde. Overall, the DSC data demonstrates that increasing the curing temperature enhances the extent of crosslinking in all formulations. However, higher bio-oil content reduces curing efficiency, as evidenced by the increased residual exothermic activity and altered thermogram shapes. These results highlight the importance of optimizing curing conditions when incorporating bio-oil to ensure adequate thermal and mechanical performance of the final resin system.

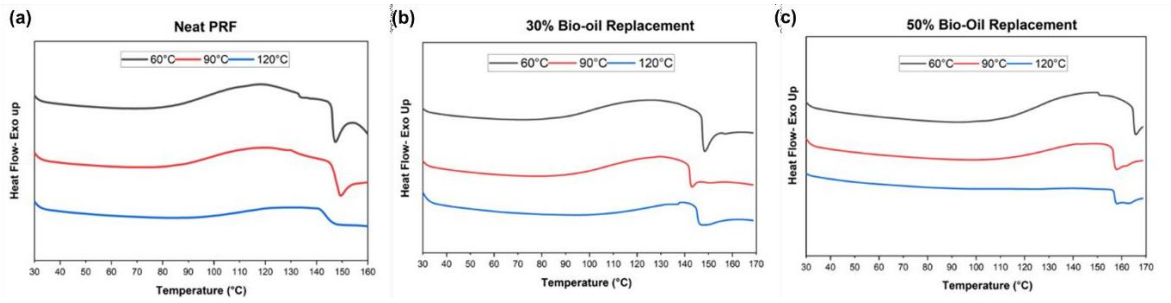

Fig. 4.4 DSC thermograms of (a) neat PRF resin, (b) 30% bio-oil replacement, and (c) 50% bio-oil replacement, after thermal curing at 60 °C, 90 °C, and 120 °C.

4.4.4.2 Flexural Response of Bio-Oil Modified PRF Resins

Figure 4.5 presents the flexural properties (flexural strength and modulus of elasticity, i.e., flexural modulus) of neat and bio-oil modified PRF resins cured at different temperatures using 10× the gelation time. Two-way ANOVA revealed statistically significant effects of formulation, curing temperature, and their interaction ($p < 0.001$) on both flexural strength and modulus of elasticity. Duncan's multiple range test further categorized the samples into distinct groups, reflecting significant differences among formulations and curing conditions.

In terms of flexural strength, the neat PRF formulation cured at 120 °C exhibited the highest values, consistent with the DSC results that showed well-defined thermal transitions indicative of a more complete curing process and a higher crosslink density. The 30% bio-oil/PRF formulation displayed intermediate flexural strength values, grouped in b or c depending on curing temperature, corresponding to the partial curing suggested by the less intense exothermic shoulder observed in DSC. Conversely, the 50% bio-

oil/PRF formulation showed the lowest flexural strength values across all temperatures (group d), reflecting the broader and more persistent exothermic transitions in the DSC thermograms that indicate incomplete and less uniform crosslinking.

Interestingly, during the 3-point bending test, the 50% bio-oil/PRF samples did not fracture but underwent extensive deformation (**Figure 4.5**), suggesting a shift toward a more ductile and flexible material. Although no fracture occurred, the maximum force recorded before the onset of large plastic deformation was used to calculate flexural strength and modulus of elasticity values, ensuring consistency in reporting while emphasizing the fundamentally different failure behavior compared to the more brittle neat PRF. This ductile behavior aligns with the low flexural strength and modulus of elasticity values, supporting the notion that higher bio-oil content reduces stiffness and promotes flexibility due to less effective crosslinking.

A similar trend was observed in modulus of elasticity values, where neat PRF cured at 120 °C demonstrated the highest stiffness (~48.8 MPa), significantly surpassing all other groups (group a). The 30% bio-oil/PRF samples exhibited intermediate stiffness (~13–15 MPa), with slight variation across temperatures (group c), while the 50% bio-oil/PRF at 120 °C showed modulus values close to zero (group d), confirming a pronounced loss of rigidity consistent with the DSC evidence of incomplete cure.

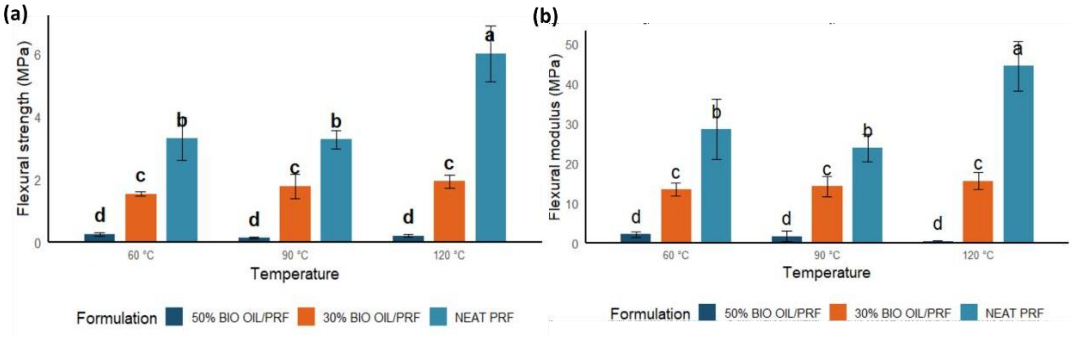

Fig 4.5 Flexural strength (a) and flexural modulus (b) of neat PRF, 30% bio-oil/PRF and 50% bio-oil/PRF formulations cured at 60 °C, 90 °C, and 120 °C, using 10× gelation time.

Note: Bars represent mean values with standard deviation (n = 4). Statistical differences were determined by Duncan's multiple range test ($p < 0.05$), with different letters indicating significantly different groups.

Figure 4.6 shows the ductile behavior of the 50% bio-oil/PRF resin cured at 60 °C, 90 °C, and 120 °C (**Figures 4.6a and 4.6b**). The samples exhibited significant flexibility without fracturing during bending tests. The specimen cured at 120 °C (**Figure 4.6c**). Displayed noticeable internal porosity, likely caused by water evaporation promoted by volatile compounds in the bio-oil during curing. This porosity may contribute to the further reduction in stiffness and strength observed in mechanical tests at higher curing temperatures. The visual evidence supports the mechanical findings, indicating that higher bio-oil content and curing temperature promote ductile behavior but also introduce defects that compromise structural integrity.

Fig. 4.6 Visual appearance of the 50% bio-oil/PRF resin specimens cured at (a) 60 °C, (b) 90 °C, and (c) 120 °C after three-point bending tests. bio-oil during the high-temperature curing process.

Note: Manually bent specimens of the 50% bio-oil/PRF formulation after three-point bending tests, cured at (a) 60 °C, (b) 90 °C, and (c) 120 °C. All samples exhibited pronounced ductile behavior, evidenced by significant bending without fracture. The specimen cured at 120 °C (c) displays visible internal porosity, which likely results from the evaporation of moisture or volatile compounds in the bio-oil during high-temperature curing. A zoomed-in detail is shown in the circle for better visualization.

These results highlight a clear trade-off between bio-oil content and mechanical performance in PRF resins. Increasing bio-oil substitution to 50% significantly reduces flexural strength and stiffness, primarily due to incomplete curing and the development of internal porosity at higher curing temperatures. However, this higher bio-oil content also imparts pronounced ductility and flexibility, as evidenced by the bending behavior without fracture. This dual effect suggests that bio-oil modified resins can be tailored for

applications requiring enhanced flexibility, but careful optimization of formulation and curing conditions is essential to minimize defects and maintain adequate structural integrity.

4.5 Conclusions

This study demonstrated that partial replacement of commercial phenol-resorcinol-formaldehyde (PRF) resin with bio-oil up to 50% significantly influences the curing behavior, thermal stability, and mechanical properties of the resulting adhesive systems. Incorporation of bio-oil slowed the curing kinetics and extended gelation times, especially at lower temperatures, although higher curing temperatures partially mitigated these effects. Thermal analysis revealed a reduction in thermal stability with increasing bio-oil content due to less thermally stable bio-oil components, yet an adequate residual char content indicated the formation of a crosslinked aromatic network. Mechanical testing showed that neat PRF cured at 120 °C exhibited the highest flexural strength and stiffness. Substitution with 30% bio-oil caused moderate decreases in these properties, while 50% substitution led to a pronounced reduction in strength and modulus, accompanied by a shift toward ductile and flexible failure behavior. This suggests that higher bio-oil content disrupts crosslink density and introduces porosity during curing. Overall, bio-oil substitution provides a promising route to partially replace phenol in PRF adhesives, enabling tunable mechanical performance and improved sustainability. However, optimizing curing conditions and formulation is critical to balance flexibility and structural integrity for targeted applications.

4.6 References

ASTM International. (2021). *ASTM D790-21: Standard test methods for flexural properties of unreinforced and reinforced plastics and electrical insulating materials*. ASTM International. https://www.astm.org/d0790-21.html

Ayrilmis, N., & Özbay, G. (2017). Propriedades tecnológicas de compensado de madeira colada com resina de resol fenol-formaldeído sintetizada com bio-óleo. *Cerne*, *23*(4), 493–500. https://doi.org/10.1590/01047760201723042351

Celikbag, Y., Nuruddin, M., Biswas, M., Asafu-Adjaye, O., & Via, B. K. (2020). Bio-oil-based phenol–formaldehyde resin: comparison of weight- and molar-based substitution of phenol with bio-oil. *Journal of Adhesion Science and Technology*, *34*(24), 2743–2754. https://doi.org/10.1080/01694243.2020.1784540

Chow, S. (1997). *26 (1972) H. 6 Thermal Analysis of Liquid-Phenol-Formaldehyde Resin Curing 229*.

Cui, Y., Hou, X., Wang, W., & Chang, J. (2017a). Synthesis and characterization of bio-oil phenol formaldehyde resin used to fabricate phenolic based materials. *Materials*, *10*(6). https://doi.org/10.3390/ma10060668

Dong, F., Wang, M., & Wang, Z. (2018). Bio-oil as Substitute of Phenol for Synthesis of Resol-type Phenolic Resin as Wood Adhesive. *International Journal of Chemical Reactor Engineering*, *16*(3). https://doi.org/10.1515/ijcre-2017-0107

Faraheen Kabir Ahmad, S., Fazara Ali, U., Isa, K., Gopinath, S. C., & K Ahmad, S. F. (2022). EVALUATION OF PHENOL FORMALDEHYDE RESIN SYNTHESIZED FROM SUGARCANE BAGASSE BIO-OIL UNDER OPTIMIZED PARAMETERS. In *Journal of Engineering Science and Technology* (Vol. 17, Issue 2). https://jestec.taylors.edu.my/Vol%2017%20Issue%202%20April%20%202022/17_2_49.pdf

Jin, F., Liu, P., Chen, L., Hua, D., & Yi, X. (2023). Study on the thermal stability of the bio-oil components by Py-GC/MS. *Energy Reports*, *9*, 280–288. https://doi.org/10.1016/j.egyr.2023.04.001

Kinnertová, E., & Slovák, V. (2018). Kinetics of resorcinol–formaldehyde polycondensation by DSC. *Journal of Thermal Analysis and Calorimetry*, *134*(2), 1215–1222. https://doi.org/10.1007/s10973-018-7532-0

Kircher, M. (2015). Sustainability of biofuels and renewable chemicals production from biomass. In *Current Opinion in Chemical Biology* (Vol. 29, pp. 26–31). Elsevier Ltd. https://doi.org/10.1016/j.cbpa.2015.07.010

Kläusler, O., Clauß, S., Lübke, L., Trachsel, J., & Niemz, P. (2013). Influence of moisture on stress-strain behaviour of adhesives used for structural bonding of wood. *International Journal of Adhesion and Adhesives*, *44*, 57–65. https://doi.org/10.1016/j.ijadhadh.2013.01.015

KOKTEN, E. S., Özbay, G., & Ayrilmis, N. (2020). Synthesis of biobased phenolic resins using catalytic pyrolysis oil and its effect on oriented strand board performance. *Journal of Adhesion*, *96*(5), 475–489. https://doi.org/10.1080/00218464.2018.1481400

Lee, W. J., Chang, K. C., & Tseng, I. M. (2012). Properties of phenol-formaldehyde resins prepared from phenol-liquefied lignin. *Journal of Applied Polymer Science*, *124*(6), 4782–4788. https://doi.org/10.1002/app.35539

Li, Q., Liu, X., Su, H., Mao, A., & Wan, H. (2020). Improving performance of phenol-formaldehyde resins modified/ blended with phenol-rich pyrolysis bio-oil. *Forest Products Journal*, *70*(4), 387–395. https://doi.org/10.13073/FPJ-D-20-00026

Liu, J., Chen, R. Q., Xu, Y. Z., Wang, C. P., & Chu, F. X. (2017). Resorcinol in high solid phenol−formaldehyde resins for foams production. *Journal of Applied Polymer Science*, *134*(22). https://doi.org/10.1002/app.44881

Liu, J., Xuan, D., Chai, J., Guo, D., Huang, Y., Liu, S., Chew, Y. T., Li, S., & Zheng, Z. (2020). Synthesis and Thermal Properties of Resorcinol-Furfural Thermosetting Resin. *ACS Omega*, *5*(17), 10011–10020. https://doi.org/10.1021/acsomega.0c00365

Meng, J., Moore, A., Tilotta, D., Kelley, S., & Park, S. (2014). Toward understanding of bio-oil aging: Accelerated aging of bio-oil fractions. *ACS Sustainable Chemistry and Engineering*, *2*(8), 2011–2018. https://doi.org/10.1021/sc500223e

Sakhakarmy, M., Kemp, A., Biswas, B., Kafle, S., & Adhikari, S. (2024). A Comparative Analysis of Bio-Oil Collected Using an Electrostatic Precipitator from the Pyrolysis of Douglas Fir, Eucalyptus, and Poplar Biomass. *Energies*, *17*(12), 2800. https://doi.org/10.3390/en17122800

Sarika, P. R., Nancarrow, P., Khansaheb, A., & Ibrahim, T. (2020). Bio-based alternatives to phenol and formaldehyde for the production of resins. In *Polymers* (Vol. 12, Issue 10, pp. 1–24). MDPI AG. https://doi.org/10.3390/polym12102237

Shahid, S. A., Ali, M., & Iqbal Zafar, Z. (2015). Bio-oil-PF resins. In *BioResources* (Vol. 10, Issue 1).

Solomon, S. O., & Rudin, A. (1990). Effects of resin and curing parameters on the degree of cure of resole phenolic resins and woodflour composites. *Journal of Applied Polymer Science, 40*(11), 2135–2149. https://doi.org/10.1002/app.1990.070401105

Sun, Y., & Sun, Y. (2020). Strong Effect of Process Parameters on the Properties of Boron-Containing Phenolic Resins with High Char Yield. *Applied Sciences*, *10*(4), 1408. https://doi.org/10.3390/app10041408

Tung, C.-Y. M., & Dynes, P. J. (1982). Relationship between viscoelastic properties and gelation in thermosetting systems. *Journal of Applied Polymer Science, 27*(2), 569–574. https://doi.org/10.1002/app.1982.070270220

Wang, M., Leitch, M., & (Charles) Xu, C. (2009). Synthesis of phenol-formaldehyde resol resins using organosolv pine lignins. *European Polymer Journal*, *45*(12), 3380–3388. https://doi.org/10.1016/j.eurpolymj.2009.10.003

Wang, X.-M., Riedl, B., Christiansen, A. W., & Geimer, R. L. (1994). Differential scanning calorimetry of the effects of temperature and humidity on phenol-formaldehyde resin cure. *Polymer, 35*(26), 5685–5692. https://doi.org/10.1016/S0032-3861(05)80042-4

Wibowo, E. S., & Park, B. D. (2024). Controlling the stability and adhesion performance of cold-setting phenol–resorcinol–formaldehyde resin adhesives through methanol addition. *International Journal of Adhesion and Adhesives*, *132*. https://doi.org/10.1016/j.ijadhadh.2024.103717

Wibowo, E. S., Park, B. D., Lubis, M. A. R., Kusumah, S. S., Santoso, A., Sari, A. A., & Iswanto, A. H. (2025). Enhancing the performance of cold-setting phenol–resorcinol–formaldehyde resin adhesives through condensation extension. *International Journal of Adhesion and Adhesives*, *138*. https://doi.org/10.1016/j.ijadhadh.2025.103958

Chapter 5

Summary and future recommendations

5.1 Summary

This research project aimed to develop, characterize, and optimize thermoset bio-composite materials using renewable fillers and partially bio-based resin matrices for their application in extrusion-based 3D printing of sustainable housing components. Across three integrated studies, the work addressed material performance at different scales—from nanoscale reinforcement to macroscale composite formulation and bio-based resin development—providing a comprehensive strategy toward sustainable construction materials.

In the first study, cellulose nanofibrils (CNFs) were explored as nano-reinforcements for epoxy matrices. Bleached CNFs (BCNF) significantly outperformed lignin-containing CNFs (LCNF) in improving toughness and stiffness, with 0.75 wt% BCNF yielding optimal mechanical properties due to better dispersion and interfacial compatibility. In the second study, wood flour–epoxy composites were optimized for extrusion by evaluating the effects of wood content, particle size, and screw speed. The 55:45 epoxy-to-wood ratio produced composites with superior strength, reduced water absorption, and improved fire resistance, confirming the critical role of formulation in performance. The third study investigated the substitution of phenol in phenol-resorcinol-formaldehyde (PRF) resins with bio-oil. Results showed that up to 30% substitution preserved thermal and mechanical performance, while higher levels introduced ductility and reduced stiffness, suggesting tunable behavior for specific applications.

Together, these studies demonstrate that bio-based fillers and partially renewable resins can be successfully integrated into high-performance composite systems for construction applications. The findings emphasize the importance of formulation optimization, filler compatibility, and process conditions in balancing mechanical performance, thermal stability, and sustainability.

5.2 Future recommendations

Future research should prioritize enhancing the production process of nanocellulose-reinforced composites to improve dispersion quality and minimize defects such as fiber agglomeration and entrapped air bubbles. Lignin-containing cellulose nanofibrils (LCNFs) present unique challenges due to their heterogeneous surface chemistry and partial hydrophobicity caused by lignin content, which often leads to poor dispersion within the epoxy matrix. This agglomeration negatively impacts mechanical performance and reduces effective fiber–matrix interaction. To address these issues, advanced dispersion techniques such as ultrasonication, or solvent exchange should be optimized and standardized during sample preparation. Additionally, careful degassing protocols should be implemented to remove air bubbles that compromise composite integrity. Improving these processing parameters will facilitate higher nanofiber loadings with uniform distribution, ultimately enhancing both mechanical and thermal properties of the composites. For the wood flour–epoxy composites developed for extrusion, further investigation into the rheological behavior during processing is essential to optimize flow characteristics and avoid defects during 3D printing. Equally important is optimizing the composite formulation to enhance the wetting and adhesion of wood flour by the epoxy resin, which directly affects dispersion quality and extrudability.

In the context of bio-oil-modified PRF adhesives, it is recommended to expand the range of substitution levels tested (e.g., 10%, 20%, and 40%) to gain a more comprehensive understanding of how bio-oil content influences curing, network structure, and mechanical properties. This broader dataset will provide better context for interpreting results and optimizing formulations. Detailed chemical and physical characterizations, including spectroscopy, rheology, and thermal analysis, should be conducted to identify reactive components and potential inhibitors. Additionally, exploring chemical modifications or hybrid curing strategies could further improve resin performance.

Across all systems, long-term durability testing under environmental exposure (humidity, UV, freeze–thaw) is necessary to validate these materials for real-world construction applications. Furthermore, life cycle assessment (LCA) and techno-economic analysis should be conducted to quantify environmental

benefits and evaluate scalability. These steps will be crucial to transition these bio-composites from lab-scale development to industrial application in the construction sector.

Appendix A

Supporting Material Chapter 2

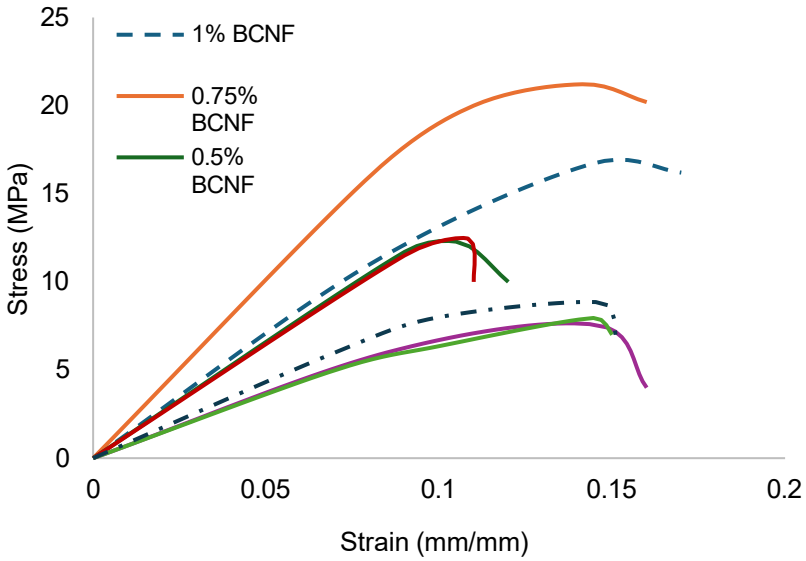

Fig. A.1 Representative Stress–Strain Curves of the Composites Used for Tensile Strength and Toughness Determination

Table A1 Maximum Tensile Strength Values of the Composites Determined from Stress–Strain Peaks

Formulation	Strain at Break (mm/mm)	Max Stress (Mpa)
1% BCNF	0.144	16.69
0.75% BCNF	0.141	21.21
0.5% BCNF	0.106	12.23
Neat Epoxy	0.108	12.46
1% LCNF	0.145	7.56
0.75% LCNF	0.145	7.95
0.5% LCNF	0.147	8.83

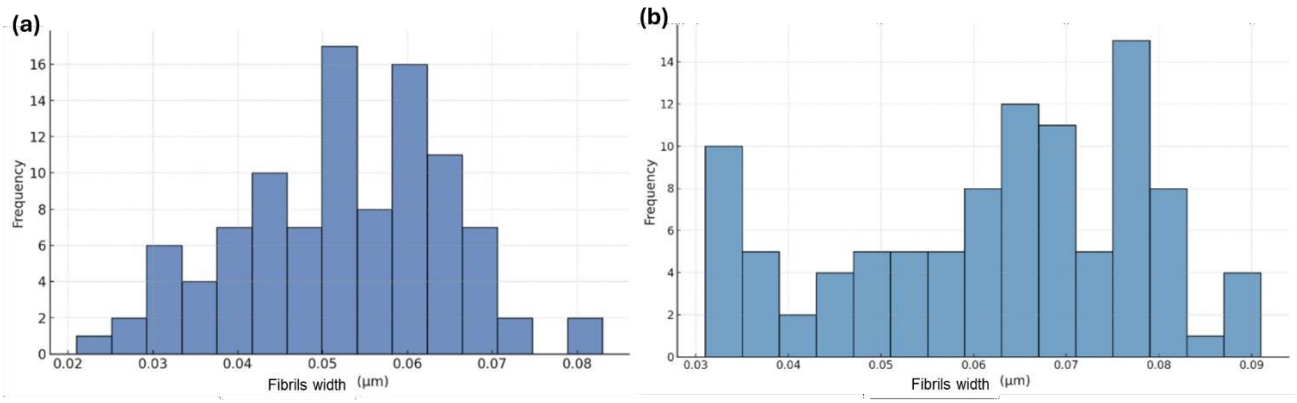

Fig. A2. Width Distribution of (a) Bleached Cellulose Nanofibrils (BCNF) and (b) Lignin-Containing Cellulose Nanofibrils (LCNF)